Arch. Metall. Mater. **63** (2018), 2, 719-738

DOI: 10.24425/122398

N. GANGIL*#, A. NOOR SIDDIQUEE**, S. MAHESHWARI*,
ABDULRAHMAN M. AL-AHMARI***, M.H. ABIDI***

STATE OF THE ART OF EX-SITU ALUMINIUM MATRIX COMPOSITE FABRICATION THROUGH FRICTION STIR PROCESSING

Aluminium metal matrix composites (AMMCs) are the fastest developing materials for structural applications. Friction Stir Processing (FSP) has evolved as a promising surface composite fabrication technique mainly because it is an eco-friendly and solid-state process. A spurt in the interest of research community and a resulting huge research output makes it difficult to find relevant information to further the research with objectivity. To facilitate this, the present article addresses the current state of the art and development in surface metal matrix fabrication through FSP with a specific focus on ex-situ routes. The available literature has been carefully read and categorized to present effects of particle size, morphology and elemental composition. The effect of various reinforcements on development of different functional characteristics is also discussed. Effect of main FSP parameters on various responses is presented with objectivity. Based on the studied literature concluding summary is presented in a manner in which the literature becomes useful to the researchers working on this important technology.

Keywords: friction stir processing; aluminium alloys; ex-situ composites

1. Introduction

Aluminium and its alloys are most widely used in many industries like aerospace, marine, transportation and structural applications because of their excellent strength to weight ratio, good formability and high corrosion resistance [1]. However, further efforts have been directed to improve its mechanical properties by various means and among most popular alternatives for this are through metal matrix composite technology which has gained momentum in the past three decades [2,3]. Al-based Metal Matrix Composites (AMMC) possess high strength, high elastic modulus, and improved resistance to fatigue, corrosion, creep and wear; which make them favourable structural materials for many industries [4-6]. Surface metal matrix composites (SMMC) are also being used recently, which are fabricated through fusion based techniques [7-17] including high energy laser melt treatment [7-12], high energy electron beam irradiation [13-14], plasma spraying [15], cast sinter [16-17] and cold spraying [18]. These techniques suffer from limitations such as formation of detrimental phases, interfacial reaction between matrix and reinforcement, and agglomeration of particles. The problems associated with above mentioned methods for MMC fabrication have focused attention to find alternate routes which is clean, simple and less time consuming than conventional methods. This gives way to a new, Friction Stir Processing (FSP) route proposed by Mishra et al. [19]. They were successful in fabricating surface composite, ex-situ, using the principle of friction stir welding [20] and their work lead to numerous researches on surface composite fabrication using FSP.

During FSW/FSP, material being processed under frictional heat is subjected to a combination of metal working processes e.g. extrusion and forging [21-26]. Under such processing conditions FSP is being used as a very effective process to modify microstructure and improve the mechanical and tribological properties at selective locations [27-28]. Compared with other metalworking techniques, FSP has many advantages such as it is a green, energy efficient, possesses short-route and it is a solid-state technique. Recently, the FSP has become popular for microstructural modification in metallic materials including superplasticity [29-34], homogenization of structure in alloys [35-37] and metal matrix composites (MMCs) [38-40], microstructural refinement of cast aluminium alloys [41-44], fatigue life improvement of arc welded joints [1, 45-46], fabrication of metal foam [47-48] and fabrication of in-situ [49-55] and ex-situ composites [2,6,19,56,60-116].

The aluminium alloys are fast subsuming other materials such as steels mainly due to their superior mechanical properties and high strength to weight ratio etc. [57-59]. There is signifi-

* NETAJI SUBHAS INSTITUTE OF TECHNOLOGY, DEPARTMENT OF MANUFACTURING PROCESSES AND AUTOMATION ENGINEERING, NEW DELHI 110078, INDIA
** JAMIA MILLIA ISLAMIA, DEPARTMENT OF MECHANICAL ENGINEERING, NEW DELHI 110025, INDIA
*** KING SAUD UNIVERSITY, ADVANCED MANUFACTURING INSTITUTE, PRINCESS FATIMA ALNIJIRIS'S RESEARCH CHAIR FOR ADVANCED MANUFACTURING TECHNOLOGY (FARCAMT CHAIR), RIYADH, SAUDI ARABIA
# Corresponding author: namrata.gangil@gmail.com

cant interest among the researchers and industry professional to develop Aluminium based SMMC to obtain several surface specific properties and the literature reports huge number of articles. There are two broad categories in which SMMC are being made namely: In-situ and Ex-situ, while there is a limited choice of suitable reinforcement materials in the In-situ route, SMMC fabrication through both the routes is complex as it involves a large number of process parameters and their effects on various important properties that are often contradictory in nature apart from the response of aluminium alloys to these process parameters themselves being embarrassingly varied and large.

There is, thus, a need to unveil the state of the art and present it in a categorical manner so that the status is reported to researchers in a systematic and holistic manner. This paper is written with this objective and focuses on the fabrication of composite on various series of aluminium alloy to know the current status of FSP process in ex-situ composite fabrication on aluminium alloys.

2. Composite fabrication on al alloys through friction stir processing

Using FSP single component reinforcement or hybrid (multiple component) reinforcement particle can be embedded in aluminium and its alloys matrix to fabricate single particle reinforced and hybrid composite in ex-situ condition. Properties of composites fabricated by such type of processing are affected by a very large number of processing parameters. One of the parameter is the strategy to pre-place the reinforcement particle over substrate and subsequently embed them via FSP. Researchers have used various techniques to pre-place the particles on substrate including pre-placed particle layer, filling reinforcements in grooves, holes and some used high velocity oxygen fuel (HVOF) technique and atmospheric plasma spraying (APS) techniques. The preplaced particles are usually packed into the substrate through an FSP run with a pinless-shoulder-tool or by using a thin Al plate before final FSP to initially cover the grooves filled with particles to prevent it from sputtering. Every aluminium alloy behaves to similar processing condition very differently simply because of varied nature of their metallurgical, structural behaviour and consequently it becomes important to understand the response of each type of alloy to the processing conditions.

2.1. Single component reinforced wrought aluminium composites

2.1.1. 1xxx Series

1xxx series of Al-alloys represents commercially pure aluminium (99% or greater), non heat-treatable, strain hardenable series having high formability, corrosion resistance and high electrical conductivity with typical ultimate tensile strength (UTS) in the range 70-185 MPa. It is extensively used in electrical and chemical applications, e.g., chemical equipments, tank, foil and strip for packaging, spun hollowware etc. [59]. The state of the art for the fabrication of ex-situ composite on 1xxx series aluminium alloys is summarized in Table 1. Dixit et al. [60] fabricated AA1100/NiTi surface composite and induced residual compressive and tensile stresses in the parent matrix using shape memory effect of NiTi particles. They investigated the effect of FSP on as-received cold rolled (CR) samples and on CR FSPed samples subjected to annealing (ANN) after FSP. They found that the phase transformations of NiTi particles induced higher residual stresses in the annealed samples (0°-10.5 MPa and 90°-17.9 MPa). CR samples showed slightly higher microhardness (57 Hv) value than ANN samples (55Hv) due to work hardening during cold reduction. Arab et al. [61] investigated the effect of FSP on AA1100 matrix by using glass and carbon fibres and reported significant increase in strength and ductility both simultaneously unlike other studies.

Several researchers have used Al 1050 alloys to fabricate surface composites through FSP route and used reinforcement as SiC (silicon carbide) [62-67], and TiC (titanium carbide) [68] to explore the improvement in its mechanical properties. It was observed by Kurt et al. [62] that shoulder diameter and tool rotational speed mainly controls the heat input and size of stir zone. The variation in thickness of Al 1050/SiC composite layer and hardness were more affected by traversing speed as compared to rotational speed. The composite layer thickness was about 150 μm and 75 μm for 15 and 30 mm/min traverse rate, respectively. The bonding of composite layer with substrate was poor at 30 mm/min. The improvement of 149% and 146% in hardness value obtained at tool traversing and rotational speed of 15mm/min and 1000 rpm and 15 mm/min and 500 rpm, respectively. Mahmoud et al. [63] used 2 mm Al sheet to initially cover the groove with SiC before FSP. BM (base metal) hardness was measured as 36 Hv. The higher average microhardness of specimen processed with 1500 rpm for first pass and 1250 rpm for second and third pass was measured 55 Hv. In some places a microhardness value of 110 Hv was observed when groove size was 3×1.5 mm. The square tool pin profile found effective for improved particle distribution, microhardness, and finer matrix grain size (1 μm) [64]. Khorrami el al. [65-67] fabricated Al 1050/SiC composite using multi-pass FSP. The two passes of constrained groove pressing (CGP) prior to FSP was conducted for imposing the intense strain of 2.32 to the Al sheets that resulted in 0.9 μm grain size and increase in microhardness from 20 Hv to 41 Hv. Initially, more homogeneous particle distribution was achieved in the advancing side (AS) as compared to retreating side (RS), as the number of FSP passes increased, particle distribution improved [65]. Initial stored strain value effect was also investigated by sheets deforming with 1, 2 and 3 CGP passes to obtain 1.16, 2.32 and 3.48 initial stored strain values, respectively. After first pass of FSP all stored energy was found to have released. SiC distribution was more homogeneous with increasing number of passes and as a result microhardness was more uniform and high at higher number of passes [66]. Stir zone

TABLE 1

A summary of ex-situ composite fabrication on 1xxx aluminium alloy

Workpiece Material	Reinforcement and Strategy	Tool specifications	Processing Parameters	Prominent Results	Reference
Al1100-H14	NiTi(2-193 μm), 1.6 mm dia. 4 holes drilled 0.9 mm below the surface.	Pin with scrolled shoulder	R-1000 rpm, T-25 mm/min, TD-2.3 mm	The shape memory effect of NiTi particles effectively induced residual stresses in matrix. Composites exhibited higher microhardness, YS and UTS.	60
Al1100	Milled and chopped Carbon, S & E glass fibre (300 μm), Groove: W-0.7 mm, D-2.5 mm	Cylindrical pin	R-1000 rpm, T-25 mm/min, TT-3°	Strength and ductility improved. Milled E GFRC exhibited highest avg. microhardness, TS, and %E of 44Hv, 105 MPa, and 46 % respectively.	61
Al1050,	SiC (10 μm), Particles mixed with methanol and applied on surface	Plain cylindrical shoulder	R-500,700,1000 rpm, T-15, 20, 30 mm/min, TT-2°, plunge depth-0.1 mm	With increasing R and decreasing T, composite layer thickness and microhradness increased. Composite showed enhanced YS and lower ductility compared to plain FSPed al alloy. Bending strength improved.	62
Al1050-H24	SiC (1.25 μm), Groove: W-2-3 mm, D-1.5-2 mm	SD-14 mm, PD-5 mm, PL-3.3 mm	R-1000-3000 rpm, T-0.83-3.33 mm/sec, TT-3°, Passes-1,2,3, Change AS&RS technique, TD-3.5 mm	Rotational speed of 1500 rpm and multipass FSP strategy were found effective for better dispersion of particles. Traversing speed had less significant effect on particle dispersion.	63
Al1050-H24	SiC (1.25 μm), Groove: W-3 mm, D-1.5 mm	SD-14 mm, PL-3.5 mm, PD-5, profiles cylindrical (3,5,7 dia) threaded, square, triangular	R-1500-2500 rpm, T-1.66 mm/sec, TT- 3°, Passes-1,2,3, change AS&RS technique	At 1500 rpm cylindrical threaded pin of 3 and 7 mm diameter could not produce sound stir zone. Square tool pin was found best among others.	64
Al1050, Annealed and CGPed 2 passes	SiC (45-65 nm), Groove: W-1 mm, D-1.5 mm	SD-12 mm, PD- 3 mm, PL- 2.1 mm	R-1200 rpm, T-50 mm/min, TT-3°, Passes-1,2,3	Hardness of composite improved 118% as compared to plain FSPed sample. Grain size refinement and reduction in agglomeration of particles with increasing passes. 1 & 2 pass specimens showed brittle fracture at retreating side due to agglomeration of SiC.	65
Al1050, Annealed and CGPed 3 passes	SiC, Groove: W-1 mm, D-1.5 mm	SD-12mm, PD- 3 mm, PL-2.1 mm	R-1200 rpm, T-50 mm/min, TT-3°, Passes-1,2,3	Al/1.5%SiC composite fabricated successfully. In SZ with sufficient SiC higher initial strain formed finer grains whereas in regions with insufficient SiC it results in grain growth.	66
Al1050, Annealed and CGPed 2 passes	SiC (55 nm), Groove: W-1 mm, D-1.5 mm	SD-12 mm, PD- 3 mm, PL-2.1 mm	R-1200 rpm, T-50 mm/min, TT-3°, Passes-1,2, Heat treatment-200, 300, 400°C for 1 hr	FSPed samples were thermally stable after heat treatment at all the temperatures. The average microhardness of FSPed specimen was found to be 42 Hv.	67
Al1050	TiC (~2 μm), Groove: W-0.5 mm, D- 5.8 mm	SD-18 mm, PD- 6 mm, PL-5.8 mm	R-1600 rpm, T-60 mm/min, AF-10 KN	Hardness was 45 % higher than BM. Peak hardness observed away from the centre of stir zone.	68
Al1016	MWCNT (30-40 nm dia, 10-20 μm length), 6 Holes-Depth- 3.5 mm, Diameter-0, 2, 4, 6, 8, 10 mm	Threaded pin pitch-0.3 mm, SD-26.8, PD-12 mm, PL-7.8 mm	R-950 rpm, T-30 mm/min, TT-2°, Passes-5	Microhardness, TS, UTS increased with increased content of MWCNT in composite. Elongation decreased with increase content of MWCNT.	69
Al1060	CNTs (outer dia-10~20 nm, length 5~15 μm), Holes: Depth-3.5 mm, Diameter-varied	—	R-950 rpm, T-30 mm/m, TT-2°	Microhardness increased with CNT content. Higher hardness observed in RS due to particle accumulation. Wear resistances improved.	70

Note: W – width, D – depth, SD – shoulder diameter, PD – pin diameter, PL – pin length, R – rotational speed, T – traversing speed, AF – axial force, TT – tool tilt, TD – target depth, BM – base metal, UTS – ultimate tensile strength, YS – yield strength, %E – Elongation.

(SZ) microstructure was thermally stable at all the temperature applied during heat treatment after FSP [67]. Thangarasu et al. [68] reported 45 % improvement in hardness value of composite using TiC as reinforcement. The Orowan strengthening mechanism was considered the major contributor for improvement in hardness [68].

Liu et al. [69] investigated the effect of 0 to 6 vol. % of multi-walled carbon nano-tubes (MWCNT) on the AA 1016

aluminium plate. TEM (Transmission electron microscopy) observations (Fig. 1) indicated high dislocation density and ultra fine-grains (50-100 nm). Elongation decreased from 26% to 9.6% with increasing content of particles in composite. The average microhardness of SZ and UTS (ultimate tensile strength) were found about 65 Hv and 192 MPa at 6 vol.% of MWCNTs with 2.2 and 2.05 times improvement, respectively, when compared to plain FSPed samples. Improvements in properties attributed to combined effect of grain refinement and strengthening effect of MWCNTs.

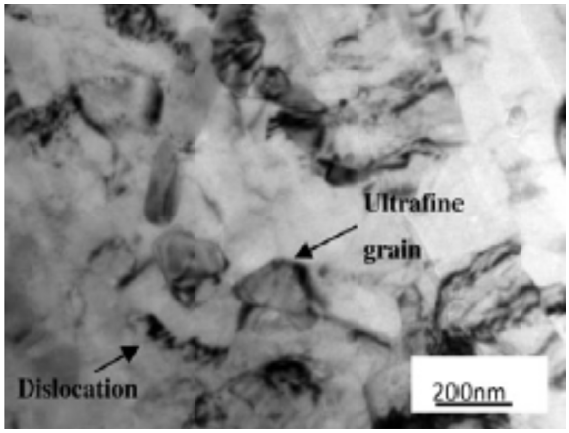

Fig. 1. TEM image showing the ultrafine grains and dislocations (reprinted with permission from the publisher) [69]

Xu et al. [70] investigated the effect of CNTs on microhardness and wear resistance on Al 1060 matrix. Maximum microhardness of 60 Hv achieved with 7 vol. % CNTs reinforcement. Wear resistance was significantly improved at 5.5 Vol. % CNTs reinforcement and results found almost unchanged at 7 Vol. % of CNTs reinforcement.

2.1.2. 2xxx series alloys

2xxx series is heat-treatable Al-Cu alloys and possess high strength at room, and elevated temperature with typical UTS range 185-427 MPa used mainly in aircraft and transportation applications. The higher strength alloys are primarily used in aircraft internal structure (AA2024) and truck body (AA2014) [59]. Table 2 summarizes the composite fabrication of 2xxx series of Al alloy. Zahmatkesh and Enayati [71] fabricated AA2024/Aluminium oxide or Alumina (Al_2O_3) surface nano-composite. Average grain size, thickness and microhardness of composite layer were found ~4 μm, 600 μm and 230 Hv, respectively. Wear resistance of composite significantly improved as average friction coefficient was found 0.31 as compared to 0.93 of BM. Wear of composite was mainly due to delamination mechanism. Sharma et al. [72] successfully fabricated AA 2014/SiC composite with improved microstructure and 87% improvement in hardness value.

2.1.3. 5xxx series alloys

Al-Mg alloys are strain hardenable and possess excellent corrosion resistance, toughness and weldability with typical UTS range of 124-352 MPa largely used in cryogenic, marine, automotive, storage tanks, pressure vessels and construction applications. AA 5083 is employed mainly in the form of machined plates for hulls, hull stiffeners, deck, and superstructure of high speed ships [59]. Table 3 summarized the fabrication of ex-situ composite on 5xxx series of aluminium alloys. AA5083 aluminium alloy has been reinforced with SiC [19, 73, 74], Al_2O_3 [75], fullerene [76], Cu [77], and ZrO_2 [78]. Mishra et al. [19] investigated the effect of traversing speed, target depth and content of SiC on the composite properties. Figure 2 shows OM images of composites. Higher value of traversing speed resulted in poor bonding of composite layer with the substrate for all value of tool plunge. Good bonding and homogeneous distribution of SiC particles occured at 25.4 mm/min traversing speed and 2.03 mm tool penetration. Composite layer thickness range was found 50-200 μm. The microhardness of BM was 85 Hv which was increased to 123 Hv at ~13 vol.% SiC and 173 Hv at ~27 Vol.% SiC.

Gandra et al. [73] investigated the effect of reinforcement particle size and tool offset on composite properties. Composite layer thickness of 80 μm observed with better particle distribution when smaller particle size was used. Effective particle distribution was achieved when tool pin offset was set to zero. Tool wear was significant when tool pin was located outside the groove. SEM equipped with EDS detected iron, Cr, Mo through surface. Grey colour showed the SiC, coarse white coloured particles are tool material inclusions (Fig. 3).

TABLE 2

A summary of ex-situ composite fabrication on 2xxx aluminium alloy

Workpiece Material	Reinforcement and Strategy	Tool specifications	Processing Parameters	Prominent Results	Reference
AA2024-T4	Pure Al (50 μm) & 10 vol. % Al_2O_3 (50 nm), APS technique	Threaded pin, SD-18 mm, PD-2.5 mm, PL-2.5 mm	R-800 rpm, T-25 mm/min, TT-3°	Average hardness increased, wear resistance improved. Al_2O_3 particles homogeneously distributed in nano-composite surface layer without any defect.	71
AA2014-T6	SiC (38 μm), Groove: W-2 mm, D-3 mm	SD-21 mm, Conical pin root dia-5 mm tip dia-3 mm, PL-3mm	R-710 rpm, T-100 mm/min, FSP passes-4	Grain size reduced from 120 μm of BM to 8 μm of SZ after FSP. Hardness of plain FSPed specimen and composite was found 80 Hv and 150 Hv, respectively.	72

TABLE 3

A summary of ex-situ composite fabrication on 5xxx series of aluminium alloy

Workpiece Material	Reinforcement and Strategy	Tool specification	Processing Parameters	Prominent Results	Refe-rence
Al 5083	SiC (0.7 μm), Particles mixed with methanol and applied on surface	—	R-300 rpm, TT-2.5°, T-25.4, 101.6 mm/min, TD-1.78, 2.03, 2.28 mm, Varying SiC %	Composite layer with well distributed particles and good bonding with Al substrate generated with mid range of selected TD (2.03 mm) and (25.4 mm/m) T. Micro hardness was found 173 Hv at higher SiC %.	19
AA5083-H111 & partially annealed	SiC (118.8, 37.4, 12.3 μm), Groove: W-1.5 mm, D-1.5 mm	Concave shoulder, threaded pin, pitch-0.3 mm, SD-18 mm, PD-7 mm	R-1000 rpm, T-25 cm /min, TT-2°, TD-2 mm, tool offset	Composite layer thickness decreases with increase in particle size due to difficulty of distribution. Effective particle dispersion was found with groove directly under pin in comparison to when groove was outside the probe	73
AA5083	SiC (35 μm, 12.5 μm), Al_2O_3 (45 μm), Two strategies: (1) pre-placed particle layer (2) Friction surfacing	For first strategy- Concave shoulder, threaded pin, SD-19 mm	Strategy 1: SiC-R-1120, 710, 355, 1800 rpm, T-180,224,355 mm/min, TT-0° Alumina-R-1120, 710 rpm, T-180, 224 mm/min, TT-0 and 2° Strategy 2: R-3000 rpm, T-348 mm/min, AF-7 kN	1st strategy was simple, feasible, less time consuming produced uniform thin layer of consolidate material with good bonding and free of voids and cracks. Particles lost to the environment. 2nd strategy is efficient in terms of particle recovery and produce thick layers though these were more heterogeneous.	74
AA5083-H111	Al_2O_3 (45μm), Pre-placed layer	—	R-1120 rpm, T-180 mm/min, Electric current-500 A DC	Depth and width of processed zone increased. Hardness drop by 10% with more uniform hardness profile compared to conventional FSP process.	75
AA 5083	Fullerene powder, Groove: W-1 mm, D-2 mm	SD-12 mm, PD 4 mm, PL 1.8 mm	R- 500-2000 rpm, T-50 mm/min, TT-3°	Hardness increased by both grain refinement and dispersion of fullerene molecules. Onion rings observed at higher R, but not at lower R due to insufficient heat input.	76
AA 5083	Cu (in micro and nano meter), Groove: W-1.2 mm, D-1.2 mm	Threaded pitch-1 mm, SD-16 mm, PD-6 mm, PL-3.2 mm	R-750, 1900 rpm, T-25 mm/min, TT-3°, Passes-4 with AS & RS change	Composite reinforced with smaller particle showed higher tensile properties and hardness at 1900 rpm. Optimum distribution achieved at 4 passes.	77
AA5083- H321	ZrO_2 (10-15 nm), Groove: W-1 mm, D-2 mm	Concave shoulder, triangular pin, SD-18 mm, PD-6 mm, PL-3.3 mm	R-800, 1000, 1250 rpm, T-40, 80, 125, 160 mm/min, TT-3°, Passes-2	Maximum hardness of 134 Hv and 10% increase in UTS were measured at 800 rpm and 40 mm/min parameters setting.	78
AA 5052-H32	Al_2O_3 (50 nm), Groove: W-1 mm, D-2 mm	SD-13.6 mm, PD-5 mm, PL-3.7 mm	R/T-8 to 100 rev/mm, TT-2.5-5°, Passes-1 to 4	Higher R/T and TT produced defect free fabrication of composite. Grain refinement, better particle distribution, and improved tensile properties observed with increasing FSP passes.	2
AA 5052	SiC (5 μm & 50 nm), Groove: W-1 mm, D-2 mm	SD-18 mm, Square Pin, PD-6 mm circum circle, PL-3 mm	R-700, 1120, 1400 rpm, T-40, 80,125 mm/min, TT-3°, Passes-4, change in rotational direction between Passes	Higher matrix grain refinement was observed with nanometer particle size. Microhardness and wear resistance improved with increasing passes and tool direction change between passes. Best particle distribution observed at 1120 rpm, 80 mm/min.	79
AA5052-H32	GO (thickness 1 nm, size 1-3 μm), pre-placed layer of GO/water colloid (15 mg/ml)	Concave shoulder SD-20 mm, PD-6 mm, PL-3 mm	R-700 rpm, T-70 mm/min, plunge depth-0.1 mm	Thermal conductivity of composite improved by 15%. Ductility is also improved.	80
AA 5059	MWCNT (30-50 nm dia, axial length 1-2 μm), Groove: W-2.5 mm, D-1.8 mm	Threaded pin, 1st pass-SD-10 mm, PD-4 mm 2nd & 3rd pass SD-12 mm, PD-5 mm	R-1130 rpm (CW), T-30 mm/min, Passes-3, 3rd pass with R-454 rpm (CCW)	Flow arm seen after 2nd passes. No flow arm after 3rd pass; particle segregation, onion ring and uniform distribution was achieved. Microhardness of 2nd pass sample –152±7 Hv, and 3rd pass sample –169±6 Hv.	81
AA 5059	Al_2O_3 (130 nm and 1.1, 4.3 μm), SiC (250 nm), B_4C (35 nm), Groove: W-4 mm, D-1.2 to 4 mm	Spiral pin for 1st pass, 3 flat pin for 2nd and 3rd pass	No. of passes-3 with different tools. 1st, 2nd pass-CCW 3rd pass-CW	With increasing passes distribution was much more homogeneous. B_4C-reinforced composite exhibits the highest hardness and tensile yield strength; however, the ductility is drastically reduced to 2.5% elongation.	82

TABLE 3. Continued

Workpiece Material	Reinforcement and Strategy	Tool specification	Processing Parameters	Prominent Results	Reference
AA 5754	Si_3N_4 (20 nm), Groove: W-1 mm, D-3 mm	—	R-1120, 1400, 1800 rpm, T-40,50,63,80,100, 160, 315 mm/min, TT-3°, plunge dpeth-0.2 to 2 mm, Passes-4	Increase in R/T increases peak temperature, SZ area and refines grains. Increasing number of passes increases SZ area. Higher T and Lower R caused higher hardness. Too high and too low tool plunge was not effective for fabrication of composite.	83
5A06 Al alloy	SiC (10 μm), Groove: W-0.5 mm, D-1 mm	Threaded pin, SD-18 mm, PD-6 mm	R-1180 rpm, T-95 mm/min, TT-2.5°, plunge dpeth-0.5 mm	Wider and deeper bulk composite fabricated successfully.	6

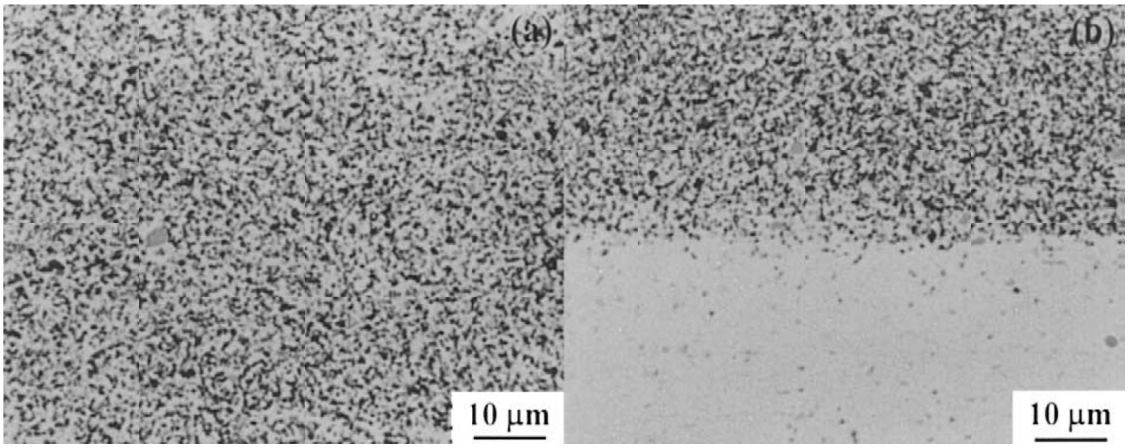

Fig. 2. OM image showing (a) uniform distribution of SiC particles (27 vol.%) in Al matrix, and (b) perfect bonding between composite layer and substrate (reprinted with permission from the publisher) [19]

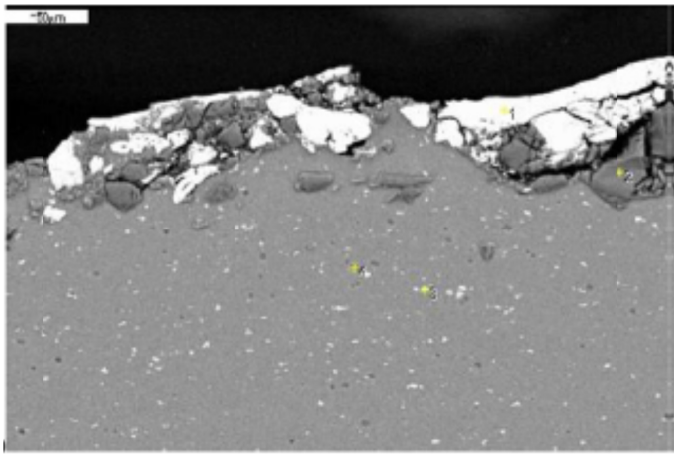

Fig. 3. SEM image of composite surface layer produced by the processing with 118.8 μm median size particles (reprinted with permission from the publisher) [73]

Miranda et al. [74] utilized two strategies, in first strategy, particles were pre-placed with spray glue and a deposition was repeated to achieve 200 μm thick layer. In second strategy, AA 6082 consumable tool of 20 mm diameter drilled with 4 holes (2 mm diameter) and filled with SiC (12.5 μm) was used. During experimentation using first strategy taking SiC and Alumina as reinforcements, effect of R/T (rotational speed/traversing speed) ratio was investigated. In Alumina reinforced composite, at R/T ratio of 6 and 3, composite track width was found 9.5 and 8.4 mm, respectively, with 204 μm deep layer. For SiC reinforced composite R/T ratio of 3 found effective with 17.2 mm track width and 133 μm deep layer. For SiC particle reinforced composite the tool wear was higher. For second strategy a parameter called RDP (ratio of deposited particles) as given in eqn-(1) was defined and expressed by volume ratio of deposited particles and consumable tool material.

$$RDP(\%) = V_{particle} / V_{rod} \times 100 = \\ = n\left(\phi_{hole} / \phi_{rod}\right)^2 \times 100 \quad (1)$$

where ϕ is diameter and n is number of drilled holes in rod. This strategy produced thick layer though these were more heterogeneous.

Santos et al. [75] were of the view that multiple pass FSP as suggested by several researchers to improve the dispersion and homogenization, is a time consuming and expensive alternative. They further reasoned that selecting high rotational speed to improve productivity would often cause the particles to disperse outside the interaction zone. So with the aim to improve the FSP process a modification using electric current assisted FSP was presented by them. It was found that the particles were uniformly distributed and well bonded with the substrate with 500% and 40% increase in reinforced zone depth and width, respectively, as shown in figure 4.

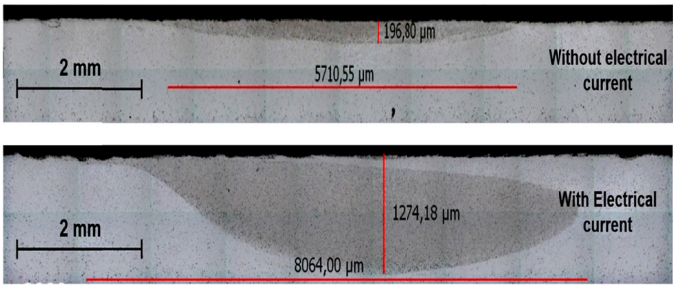

Fig. 4. Macrographs of cross sections of composites. AS and RS are on the left and right hand sides, respectively (reprinted with permission from the publisher) [75]

Morisada et al. [76] observed that the formation of onion ring and heat input were closely related. From OM images in figure 5 it was clear that the flow was convectional and shoulder driven and occurs at higher rotational speed due to enough area of plastic flow zone. Matrix grain size refined to ~200 nm with 143 Hv at 1500 rpm using fullerene dispersion.

Zohoor et al. [77] used four number of FSP passes with variable AS and RS technique for better dispersion. UTS and microhardness values were higher for nano composites at higher rotational speed which are approximately 365 MPa and 134 Hv, respectively [77]. Shahraki et al. [78] reported that at lower rotational speed (800 rpm) and higher traversing speed (160 mm/min) improper particle distribution and agglomeration of particles occurred due to insufficient stirring. SEM images (Fig. 6) showed that pores between ZrO_2 and matrix gradually diminished when R/T ratio increased due to uniform dispersion of ZrO_2 in matrix and high frictional heat generation. UTS and Microhardness improved by about 10 and 30%, respectively, mainly due to grain size reduction.

The alloys AA 5052 has also been reinforced with variety of reinforcement including Al_2O_3 [2], SiC [79], and GO (graphene oxide) [80]. Sharifitabar et al. [2] found various defects such as large voids and tunnels at low tool tilt and R/T ratios, these defects were also present with higher R/T ratio. The SZ mean grain size found was 940 nm. With increased passes the mean clusters size reduced from 650 nm in one pass to 70 nm in four passes and tensile strength improved. Dolatkhah et al. [79] reported that the shifting the rotation direction overcame the tendency of agglomeration of powder in AS (Fig. 7). Matrix grain size decreased as the number of passes increased. When SiC of 5 µm size was used matrix grain size reduced to 4.2 µm without shift in rotational direction, while shifting the direction it reduced to 2.2 µm. For SiC of 50 nm size matrix grain size reduced from 2.2 to 0.9 µm and the highest hardness of 116 Hv achieved with 9.7 % reduction in wear rate as compared to BM.

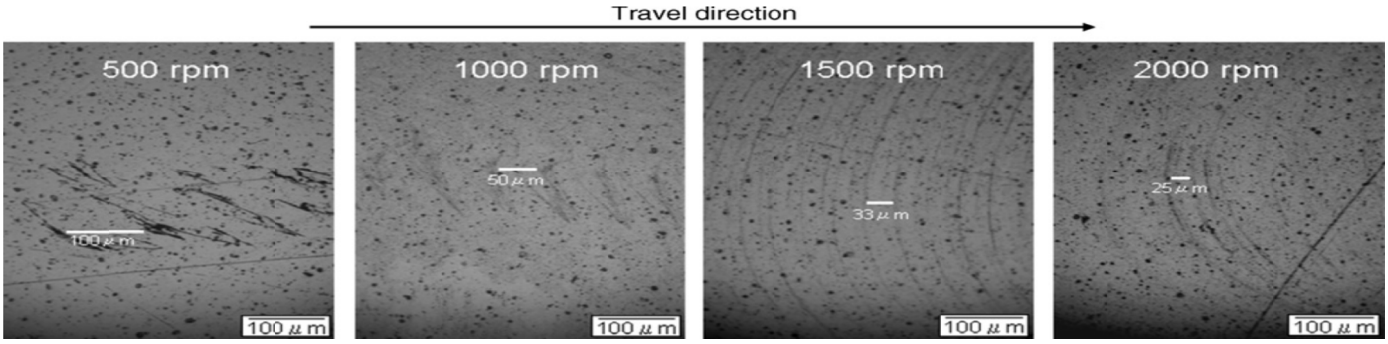

Fig. 5. OM images of the lateral sections for the FSPed samples with the fullerene at various rotating speeds (reprinted with permission from the publisher) [76]

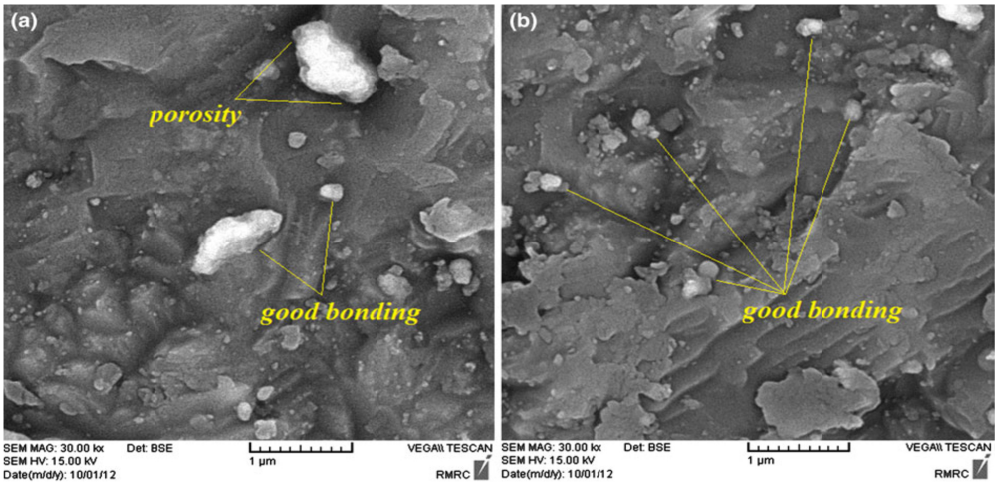

Fig. 6. SEM images showing porosity and good bonding at (a) 800 rpm, 80 mm/min; (b)1250 rpm, 80 mm/min (reprinted with permission from the publisher) [78]

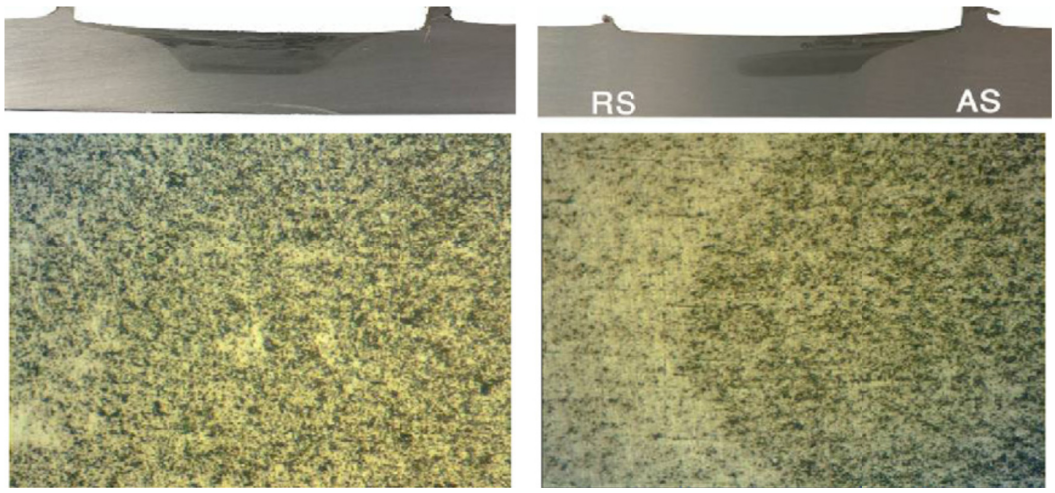

Fig. 7. SiC particle distribution in specimens FSPed with (a) 4 passes with change of rotational direction between passes and (b) without that change (reprinted with permission from the publisher) [79]

Jeon et al. [80] fabricated Al/Graphene composite to provide benefits in development of heat exchanger. Thermal conductivity of composite improved by 15 % at 250°C due to reduction of GO to highly conductive RGO with improved ductility.

Izadi and Gerlich [81] investigated the dispersion and structure survivability of MWCNTs in AA 5059/MWCNT composite. After 2nd pass of FSP the grain size was found 1 to 2 μm with survived CNTs (tubular structure), and after 3rd FSP pass it was 200 to 500 nm with no survived CNTs (polyaromatic carbon structure). Identification from SEM and TEM images revealed that 23±2.5 and 52±2.1 vol. % of reinforcing particles contained in 2nd and 3rd FSP pass samples, respectively. Higher concentration of reinforcement in 3rd pass sample attributed to variation in powder packing and increasing penetration of tool but strengthening contribution was lower because structural changes of CNTs. Sahraeinejad et al [82] fabricated surface composites using SiC (nm), Al_2O_3 (micro and nano meter) and B_4C (nm) reinforcements. With 4.3 μm sized Al_2O_3 reinforcement FSP results in more refinement of particles and composite includes 72% of <0.5 μm particles which was significantly higher than the 55% of <0.5 μm particles when composite fabricated using 1.1 μm sized Al_2O_3. B_4C reinforced composite exhibited highest microhardness (170 Hv) and yield strength (290 MPa) [82].

Moghaddas and Bozorg [83] fabricated AA 5754/Si_3N_4 composite and investigated the effect of rotational speed, traverse rate, tool plunge and number of passes on composite properties. The highest hardness achieved was 80 Hv, nearly doubled the hardness of as-received material.

Wang et al. [6] and fabricated bulk 5A06Al (in Chinese standard)/SiC composite successfully and found good interface conditions between particles and matrix. Reinforced region width became narrower with increasing depth. On the depth of 0.5 and 1 mm microhardness improvement was 10%. In SEM image (Fig. 8) point A represents good interface bonding, B-kiss bonding, C-worst bonding or impurity [6]. A similar kind of kissing bond was also observed by Khan et al. [24] in FSW joints of dissimilar aluminium alloys.

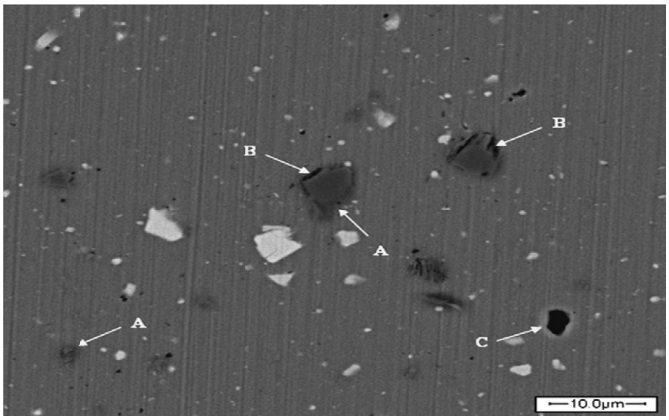

Fig. 8. SEM backscattered electron image of interface in SZ (reprinted with permission from the publisher) [6]

2.1.4. 6xxx series alloys

Al-Mg-Si alloys are heat-treatable having UTS range of 124-400 MPa with excellent extrudability and high corrosion resistance. They are largely used in marine, automotive, building and construction and highway applications [59]. Table 4 summarized the fabrication of ex-situ composite on 6xxx series of aluminium alloys. Zarghani et al. [84,85] fabricated 6082 Al/Al_2O_3 composite and investigated the effect of number of FSP passes. Dark region in SEM image (Fig. 9) of one FSP pass sample showing clustered Al_2O_3 particles (0.1 to 2 μm) and white colour showing strengthening precipitates. Cluster size, Al grain size, zener limiting grain size, and microhardness after four passes were 90 nm, 0.66 μm, 0.40 μm, and 295 Hv, respectively [84]. While in their second study these were 76 nm, 0.48 μm, 0.34 μm, and 312 Hv, respectively. The dominant wear mechanism of composite layer was abrasive at 20 and 40 N applied load, however, at 60 N applied load it was dominated by adhesive and slightly severe wear [85]. Thangarasu et al. [86] used TiC reinforcement particles and observed that the stir zone area decreased from 65 mm^2 at 0 vol.% to 34 mm^2 at 24 vol.% of

TABLE 4

A summary of ex-situ composite fabrication on 6xxx series of aluminium alloy

Workpiece Material	Reinforcement and Strategy	Tool Specifications	Processing Parameters	Prominent Results	Reference
AA 6082	Al_2O_3 (50 nm), Groove: W-1 mm, D-4 mm	SD-16 mm, PD-5 mm, PL-4 mm	R-1000 rpm, T-135 mm/min, TT-3°, Passes-1 to 4	Microhardness, wear resistance, and grain refinement increased with FSP passes and better distribution of Al_2O_3 particles achieved. Friction coefficient was found 0.35 at 60N load.	84
AA 6082	Al_2O_3 (50 nm) Groove: W-1 mm, D-4 mm	SD-16 mm, PD-5 mm, PL-4 mm	R-1250 rpm, T-135 mm/min, TT-3°, Passes-1 to 4	Friction coefficient was found ~0.37, 0.4, and 4.3 for the applied load of 60, 40 and 20N, respectively.	85
AA 6082	TiC (~2 µm), Groove: W-0, 0.4, 0.8, 1.2, 1.6 mm, D-5 mm	Threaded pin, SD-18 mm, PD-6 mm, PL-5.5 mm	R-1200 rpm, T-60 mm/min, AF-10 kN,	Microhardness and UTS of 0 and 24 Vol. % of TiC was 62 Hv and 222 MPa, and 149 Hv and 382 MPa, respectively. The wear rate was observed $693x10^{-5}$ mm^3/min at 0 vol. % and $303x10^{-5}$ mm^3/min at 24 vol.% of TiC.	86
AA6061-T651	SiC (300 nm), Al_2O_3 (200 nm), Various surface reservoir patterns	Threaded pin profile, SD-19.05 mm, PD-3.35 mm, PL-4 mm	R-1000-1800 rpm, T-0.1-1 mm/sec, T6 heat treatment of Al-alumina composite after FSP	The Al/SiC composite exhibited comparatively higher hardness (1.33±0.17 GPa, 1.96 N) than others. T6 heat treated composite exhibited lowest wear rate of $(4±0.8)×10^{-4}$ mm^3/Nm.	87
AA 6061	SiC (50 nm), Groove: W-1 mm, D-5.9 mm	Threaded & square Pin, SD-20 mm, PD-7.8 mm, PL-6 mm	R-800, 1000, 1200, 1600 rpm, T-40, 80, 125, 160 mm/min, plunge depth-0.12, 0.18, 0.24, 0.3	Parameters settings at 1600 rpm, 40 mm/min, 0.3 mm with threaded pin gave higher TS. R found to be most influencing parameter (43.7% contribution) followed by T, Pin, TD.	88
AA6061	SiC, Groove: W-2 mm, D-1 mm	—	R-1600 rpm, T-80 mm/min, pass-2, Varied AS&RS	Homogeneous particle distribution and fine grained structure observed. Composite exhibited improved hardness as compared to plain FSPed specimen.	89
AA 6061-T6	SiC (50 nm), Groove: W-3 mm, D-5.9 mm, after fabrication additional groove made with W-5 mm, D-2 mm	Threaded pin, SD-20 mm, PD-7.8 mm, PL for homogeneous composite 6mm, for FG composite 3.2 mm	R-1600 rpm, T-40 mm/min, TT-3°, Passes-4 for Homogeneous composite, additional 4 with FG	Surface hardness and friction coefficient of homogeneous and FG composite are 140 Hv, 0.8 and 155 Hv, 0.7, respectively. The FG composite showed higher work of fracture than the homogeneous composite.	90
AA6061	SiC (50 nm), Groove: for homogeneous composite- W-5 mm, D-5.9 mm; For FG composite- W-3 mm, D-5.9 mm; after FSP, W-2 mm, D-2 mm	Threaded pin, SD-20 mm, PD-7.8 mm, PL-For homogeneous composite 6 mm, for FG composite 3.2 mm	R-1600 rpm, T-40 mm/min, TT-3°	Hardness of homogeneous and FG composites were 135 Hv and 160 Hv, respectively. It decreases with depth in FG composite due to decrease in SiC vol. %.	91
AA 6061	Al (~45 µm), Al_2O_3 (10 µm), Cold gas dynamic spraying	—	R-894, 1723 rpm, T-88 mm/min, TT-3°, coating thickness varies with 29 to 90 wt.% Al_2O_3	The highest volume fraction of Al_2O_3 obtained in MMC was 48 wt.% when 90 wt.% Al_2O_3 was used. Hardness of this coating increased from 85 to 137 Hv at 894 rpm.	92
AA6061	Al_2O_3 (320 nm), Holes: Depth- 2mm, Diameter- 1mm	SD- 12.5 mm, PL-2mm, threaded conical pin three flat sides	R-1200 rpm, T-3 mm/sec, TT-2.5°, AF-3.6-4.2KN (Not varied), Passes-4	Microhardness, UTS, YS, %E of BM were 55±3 $HV_{0.5}$, 125 MPa, 55 MPa, 25% which were increased to 103±2 $HV_{0.5}$, 228 ±5 MPa, 111±3 MPa, 24±1 %, respectively, for 4 FSP pass composite.	93
AA 6061	B_4C (~5-7 µm), Groove: W-1 mm, D-2 mm	Concave shoulder SD-14 mm, PD-5 mm, PL-2.7 mm	R-1200 rpm, T-100 mm/min, TT- 2.5°, FSP passes-1,2,3,4	Four pass FSP sample showed homogeneous distribution, superior microhardness and wear properties. Highest average microhardness and lowest friction coefficient were 98 Hv and 0.35, respectively.	94
Al6061-T651	$Ni_{49.5}Ti_{50.5}$ (150-178 µm and 2-74 µm), Holes: Diameter 4 mm, Depth-5 mm	Threaded pin, SD-24 mm, PD-8 mm, PL-4.8 mm	R-600 rpm, T-100 mm/min, TT-2.7°, plunge depth-0.2 mm, Passes-4, T-6 Heat treatment and aging.	The composite reinforced with small sized particles exhibited higher strength than with large one. Heat treated composites reinforced with small sized particles exhibited higher strength than the as-received material.	95

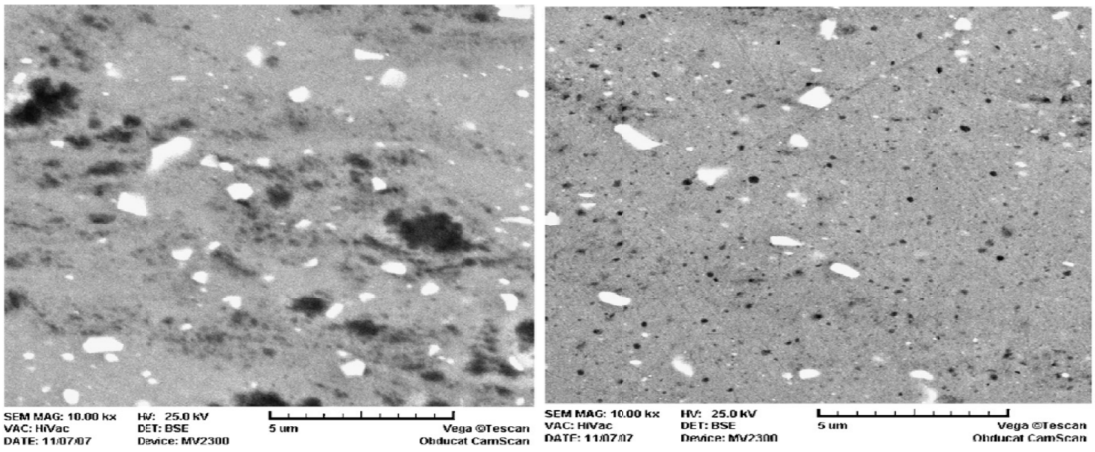

Fig. 9. SEM images composite layers produced by (a) one, (b) four FSP passes (reprinted with permission from the publisher) [84]

TiC. No change in TiC particles size and morphology reported, which was attributed to their initial small size. Wear behaviour of the composites indicated that the wear mechanism gradually changed from adhesive to abrasive with increased volume fraction of TiC [86].

AA6061 aluminium has been fabricated with variety of reinforcements including SiC [87-91], Al_2O_3 [87, 92, 93], B_4C [94], NiTi [95]. Qu et al. [87] successfully fabricated 25 and 30 vol. % of Al_2O_3 and SiC reinforced surface composites, respectively, with 2-3 mm thickness of layer. A subsequent T6 heat treatment further enhanced the wear resistance by 30%.

Salehi et al. [88] applied Taguchi method and ANOVA (analysis of variance) for the analysis. At the optimum combination of parameters they obtained highest UTS of 153.7 MPa, formation of onion ring and 4 vol. % SiC particles in composite. The increase in strength was attributed to strengthening mechanisms such as Orowan, enhanced dislocation density and grain refinement [88]. Choi et al. [89] reported the average hardness of samples FSPed without and with SiC were 55 and 75 Hv, respectively. Saadatmand and Mohandesi [90] fabricated FG (functionally graded) composite and found that the grain size of FG composite was lower than the homogeneous composite. The volume fraction of SiC was 16 % in both the composites. The figure 10a shows that the rate of wear increased with applied load. Figure 10b shows the microhardness and volume fraction of SiC along the depth has followed the same curve. FG composite showed higher wear resistance for all applied loads, higher work of fracture and increased resistance to microgalling [90]. Salehi et al. [91] found that the Mean cluster size of FG and homogeneous samples was 68±39 and 88±40 nm. Inter particle spacing values for homogeneous and FG composites with 5.5 wt.%, 10 wt.%, and 18 wt.% SiC layer was found 133.3, 271, 183.5, and 117 mm, respectively. The plot of microhardness versus inverse of interparticle spacing is shown in figure 11. It was found that microhardness value increased with decrease in inter particle spacing [91]. Hodder et al. [92] embedded more than 40 wt.% Al_2O_3 in substrate. The average particle size for 17 and 48 wt.% Al_2O_3 in as-sprayed coating were found 8±3.6 μm^2 and 4±1.7 μm^2, respectively, whereas after FSP at 894 rpm it reduced to 2±0.9 μm^2, which resulted in decrease of mean free inter-particle spacing and improvement in hardness of composite [92].

Guo et al. [93] pre-placed a mixture of dolapix CE64 (used as a dispersant) alumina and deionised water in holes which was followed by drying and friction stir processing. They observed significant improvement in microstructure and tensile properties.

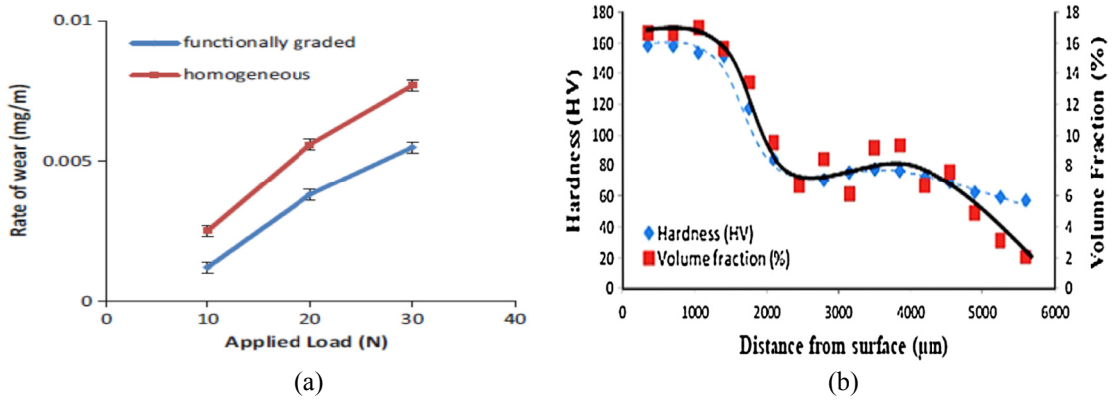

Fig. 10. (a) The rate of wear as a function of applied load, (b) Microhardness and volume fraction of SiC (%) as a function of distance from the surface of the FG composite (reprinted with permission from the publisher) [90]

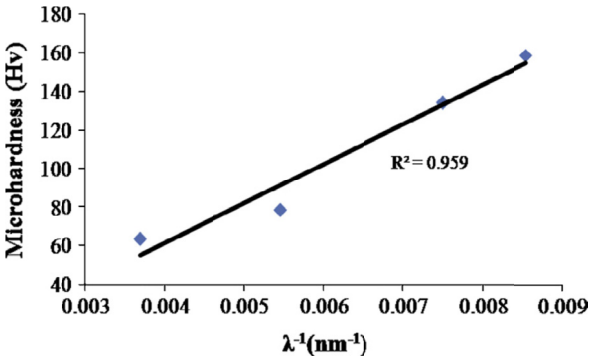

Fig. 11. Microhardness vs. the inverse of interparticle spacing (reprinted with permission from the publisher) [91]

The finer grain size of composite zone (2.5 μm) was attributed to Zener Pinning Effect. The EBSD analysis measured higher fraction of low angle grain boundaries (LAGBs). The strengthening contribution of the grain size difference (calculated from Hall Petch equation) and Orowan strengthening (due to finely dispersed nano-alumina particles calculated from modified Orowan equation) were 12.5 and 47 MPa, respectively. Orowan strengthening was found as a major contributor in improvement of tensile properties [93]. Zhao et al. [94] investigated the effect of FSP passes on hardness and wear resistance using B_4C as reinforcement. In macrographs (Fig. 12) of one and two pass specimen arrow pointed dark region showing accumulated B_4C particles, while with three and four FSP passes no accumulation appeared which resulted in significant improvement in microstructure and composite properties.

Like the studies conducted for AA 1100 [60-61] on fabricate of composites by using shape memory alloys (SMAs) particles Ni et al. [95] also fabricated Al6061/NiTi bulk composite with good shape memory effect (SME) and mechanical properties in order to achieve its wide application as sensors or actuators. They reported that the small NiTi reinforced composite showed higher strength as compared to large one. It was found that besides the one-way-SME, composite can also exhibit two-way-SME.

2.1.5. 7xxx Series alloy

Al-Zn alloys are heat-treatable possess very high strength (UTS range-221 to 607 MPa), and high toughness used mainly in aerospace and automotive applications [59]. A summary of composite fabrication on 7xxx series of aluminium alloys is given in Table 5.

AA7075 was reinforced with variety of reinforcement including MWCNTs [96], SiC [56, 97], TiN [98] and B_4C [99]. Lim et al. [96] used 1.1 mm thick sheet of AA 6111-T4 as a cover plate for CNTs used as reinforcement. There was limited inter-diffusion of top and bottom sheet and alternating lamellae was produced. They found that, for up to 1500 rpm, the CNTs segregated along the lamellae region in SZ and a non-uniform hardness was also observed, but when rotational speed increased

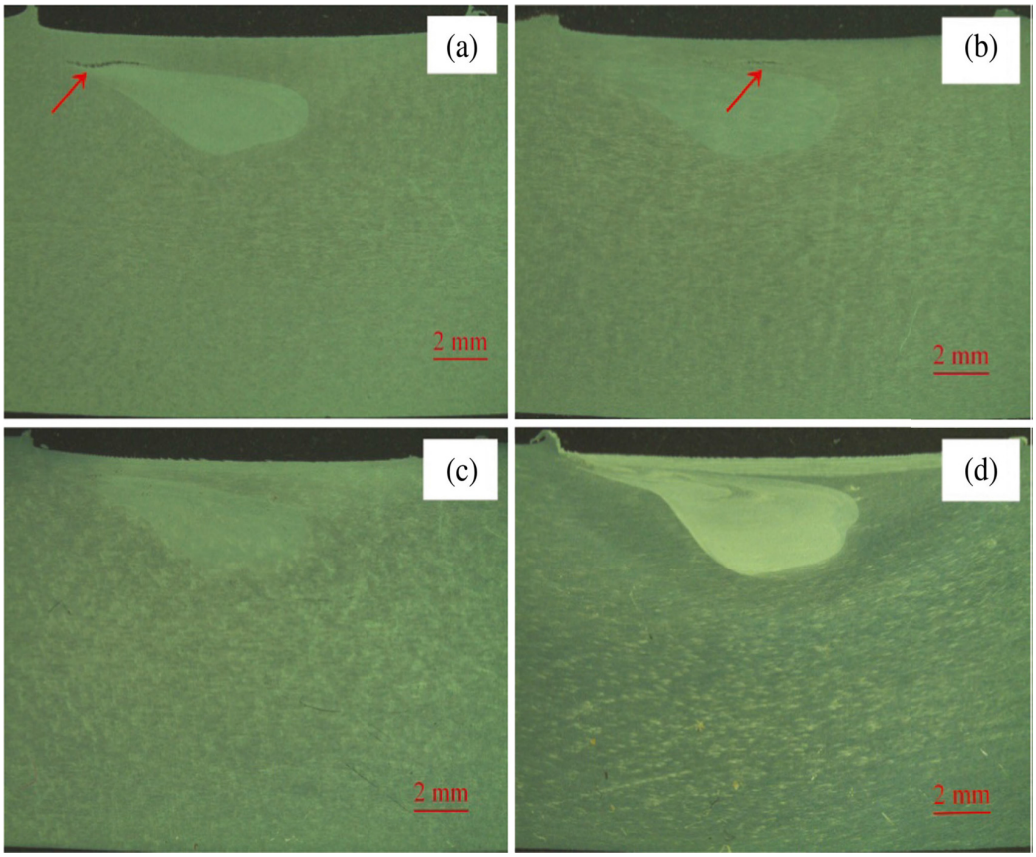

Fig. 12. Macroscopic images of the cross section of composite produced by (a) one, (b) two, (c) three, and (d) four FSP passes (reprinted with permission from the publisher) [94]

TABLE 5

A summary of ex-situ composite fabrication on 7xxx series of aluminium alloy.

Workpiece Material	Reinforcement and Strategy	Tool specifications	Processing Parameters	Prominent Results	Reference
Al7075-T6	MWCNT (30-50 nm diameter, length-10-20 µm), Groove: W-0.3 mm, D-2.3 mm	Threaded pin, SD-10 mm, PD-4 mm, PL-2.2 mm	R-1500-2500 rpm (CCW), T-2.5 mm/sec, plunge depth-0.03-0.24 mm	Homogeneity and particle distribution improved with increasing parameter values. For more homogeneous particle distribution multi pass FSP suggested.	96
Al7075-O	SiC (45-65 nm), Grooves: W-0.2 mm, D-5 mm	Threaded tapered pin, SD-16mm, PL-5.7 mm	R-800, 1000, 1250 rpm, T-30.5,40,50 mm/min	At high value of R particle dispersion improved. Higher R and intermediate T showed superior UTS and %E.	97
AA7075-0	SiC (80 nm), Grooves: two types-1st-Single (W-1 mm, D-1.5 mm), 2nd- three gradient (W-1 mm, D-0.3, 0.5, 0.7 mm)	Triangular pin, SD-22 mm, PD-10 mm, PL-1.5 mm	R-1250 rpm, T-100 mm/min, TT-3°, Passes-1, 4, 8, Variable AS & RS technique	Three gradient groove strategy resulted in most uniform particle distribution. Hardness values found less scattered as compared to other techniques.	56
Al7075-T651	TiN (30 nm)	SD- 16 mm, PL-3 mm, PD-5 mm, Pin-square, triangular, threaded tapered (tip dia-3 mm)	R-1250 rpm, T-40 mm/min, TT-2.5°, plunge depth-0.2 mm, FSP passes-2,4	Threaded tool better distributes the particles. Lowest grain size, highest hardness and wear resistance improvement obtained were 1.4 µm, 173 Hv, 60%, respectively, with 4 FSP passes and threaded tapered pin.	98
AA7075	B_4C (160, 60, 30 µm)	Threaded pin profile, PL-3 mm	R-1000 rpm, T-50 mm/min, plunging speed-30 mm/min	Microhardness and Ballistic resistance improved. Microhardness and DOP of BM, Al/B_4C-160 µm, Al/B_4C-60 µm, Al/B_4C-30 µm reinforced composites were 90, 140, 190, 260 VHN and 34, 30, 29, 24 mm, respectively.	99

from 1500 to 2500 rpm distribution improved due to increased number of lamellae. They demonstrated through a micro-hardness study (Fig. 13) that the hardness across the line C-C was more uniform compared to bulk of SZ with an average value around 170 Hv because CNTs transferred to this region by pin threads and was concentrated there.

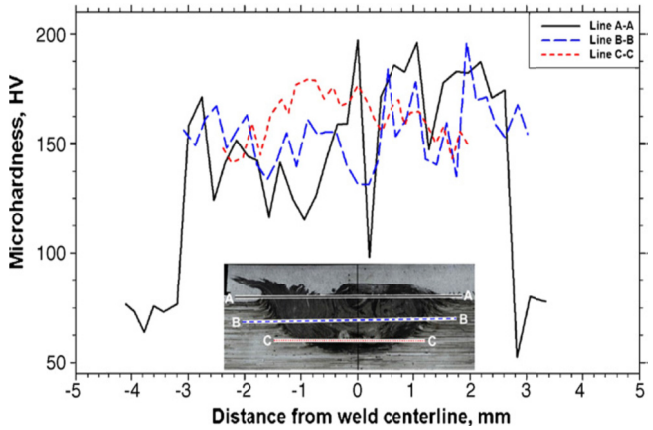

Fig. 13. Hardness measurements in a sample produced using 2500 rpm, and a 0.24 mm plunge depth (reprinted with permission from the publisher) [96]

Behrami et al. [97] fabricated AA 7075/SiC nano-composites and investigated the effect of rotational and traversing speed on composite properties. At optimum setting of tool rotational and traversing speed of 1250 rpm and 40 mm/min the UTS, average microhardness, % elongation, and grain size were 270 MPa, 111.4 Hv, 10.04%, and 3.85 µm, respectively. Heydarian et al. [56] fabricated SiC surface composites by applying three-gradient grooves method and compared it with single groove strategy with same SiC volume fraction using aligned passes and variable AS and RS strategy. They demonstrated through macrograph (Fig. 14) and micrographs that powder accumulation occurs in the AS as a result of "maelstrom current" in single groove aligned pass samples. Less accumulation and uniform dispersion of powder was obtained (Fig. 15a) when they used a strategic variable AS and RS technique. Three-gradient grooves strategy resulted in wide composite zone and uniform powder distribution in both AS and RS (Fig. 15b) and this composite showed least fluctuation in microhardness.

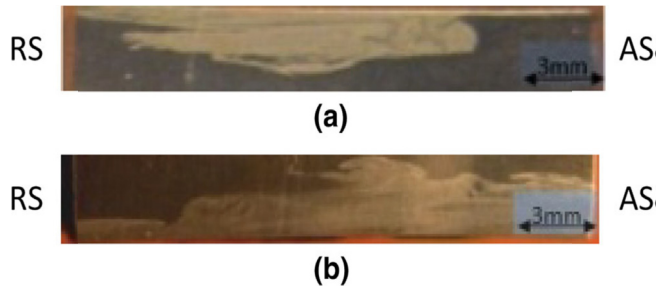

Fig. 14. Macro-images (a) four-pass specimen and (b) eight-pass specimen (reprinted with permission from the publisher) [56]

Threaded tapered tool pin profile at 4 FSP passes found effective to fabricate AA 7075/TiN composites. Un-reinforced

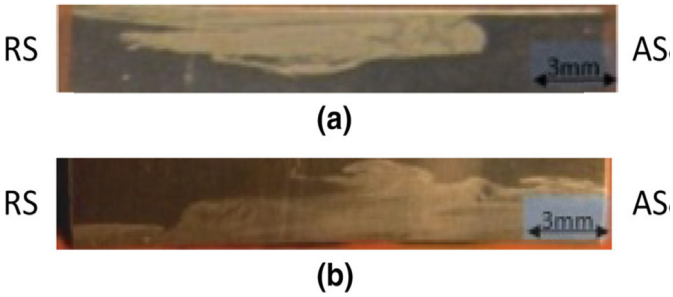

Fig. 15. Macro-image of specimens produced by (a) ''variable AS and RS'' technique, (b) ''three-gradient grooves'' technique (reprinted with permission from the publisher) [56]

FSPed samples showed annealing effect due to FSP, whereas reinforcement with TiN particles overcomes this effect. Subsequent to the wear test the EDS of worn surfaces depicted the presence of Al_2O_3 and Fe_3O_4 particles which alter the wear system to three bodies, resulted in further improvement of wear resistance of composite [98]. Sudhakar et al. [99] enhanced the ballistic resistance of AA 7075 by compositing it with B_4C particles (160, 60, 30 µm) and developed an analytical model for predicting penetration depth. Highest hardness and lower DOP (degree of penetration) was obtained when surface composite reinforced with 30 µm B_4C particles.

3. Hybrid composites fabricated on wrought aluminium alloys

When matrix is reinforced with two or more reinforcement then the resultant microstructure is termed as hybrid composite. Table 6 summarized the fabrication of ex-situ hybrid composite on wrought aluminium alloys. Mahmoud et al. [100] investigated the effect of different hybrid ratios (Al_2O_3/SiC) on hardness and wear properties. They detected small voids around Al_2O_3 particles of composites with higher Al_2O_3 contents. The maximum hardness (60 Hv) was found with 100% SiC composite which decreased almost linearly with an increase in the relative amount of Al_2O_3 content in the composite to a value of 47 Hv at 100% Al_2O_3. They reported that the wear volume loss reduced due to addition of reinforcement especially at low loads. Wear volume loss was lowest for 20 vol.% Al_2O_3 hybrid ratio composite at 5 N load because these particles had solid lubricating effect. At 10 N load the wear volume loss was not affected by hybrid ratio and showed severe wear. Soleymani et al. [101] fabricated AA5083/(SiC+MoS_2) composite layer of 2.1 mm thickness. Hybrid composite revealed highest wear resistance (Fig. 16) and maximum hardness (102 Hv) obtained with Al/SiC composite. The wear mechanism of hybrid composite was light delamination-light abrasion.

TABLE 6

A summary of hybrid composite fabrication on wrought aluminium alloys

Workpiece Material	Reinforcement and Strategy	Tool Specification	Processing Parameters	Prominent Results	Reference
Al-1050-H24	SiC, Al_2O_3 (1.25 µm), Groove: W-3 mm, D-1.5 mm, Al sheet 2 mm thick to cover sheet	SD-14 mm, PD-6 mm, PL-3.3 mm, Square pin	R-1500 rpm, T-1.66 mm /sec, TT-3°, Powder vol. %, Passes-2, 3. Variable AS&RS technique	Wear resistance improved, especially at relatively low loads. Average hardness increased about 3 times at 100 vol.% of SiC and decreased with increasing Al_2O_3 vol.%.	100
AA5083	SiC, MoS_2 (5 µm), Mixture Weight ratio-2:1, Groove: W-0.65 mm, D-2 mm	SD-20 mm, PD-6 mm, PL-2.8 mm, Square pin	R-1250 rpm, T-50 mm/min	Hybrid composite showed highest wear resistance followed by Al/MoS_2 and Al/SiC. Al/SiC composite showed highest hardness followed by hybrid composite and Al/MoS_2.	101
AA5083-H116	Al_2O_3 (80 nm), Gr (10-50 µm), Groove: W-1 mm, D-4.5 mm	SD-18 mm, PD-6, PL-5 mm, threaded pin	R-1250 rpm, T-20 mm/min, TT-3°, FSP Passes-3, Different hybrid ratio	Hardness, YS and UTS increases with Al_2O_3 hybrid ratio up to 50%, decreases at higher %. Wear rate decreases with Gr hybrid ratio up to 75% and increases at higher %.	102
AA5083	CeO_2 (30 nm), CNTs (10-20 µm length, 10-20 nm diameter), Groove: W-1.2 mm, D-2 mm	Concave shoulder, threaded pin, SD-18 mm, PD-6 mm, PL-4.5 mm	TT-5°, No. of FSP pass-3, for 1st two passes R-800 rpm, T-35 mm/min. 3rd pass-R-600 rpm, T-45 mm/min, Different hybrid ratio	Maximum TS and hardness observed are 396 MPa, 173 VHN for 75/25 CNT/CeO_2 reinforced composite with 42% increase in TS and 118% increase in hardness. Best corrosion resistance with CeO_2 reinforced composite. CNT reinforced composite shows lowest resistance.	103
AA6360	TiC (2 µm), B_4C (3 µm), Groove: W-0.5 mm, D-5.5 mm	Threaded pin, SD-18 mm, PD-6 mm, PL-5.8 mm	R-1600 rpm, T-60 mm/min, AF-8KN; Passes-2 in opposite direction, different hybrid ratio	Equal volume content reinforced composite showed lowest wear rate due to formation of tribo film.	104
AA6061	SiC, Gr, Al_2O_3 (20 µm), Groove: W-3 mm, D-3 mm	SD-24 mm, PD-8 mm, PL-3.5 mm, threaded tapered pin	R-900 rpm, T-40 mm/min, AF-5kN, TT-2.5°, SiC + Gr or Al_2O_3 -8:4 vol. %	Al/SiC+Gr composite showed lower hardness, superior wear properties than Al/SiC+Al_2O_3.	105

TABLE 6. Continued

Workpiece Material	Reinforcement and Strategy	Tool Specification	Processing Parameters	Prominent Results	Reference
AA6061	SiC, Gr, Al_2O_3 (20 µm), Groove: W-2 mm, D-3 mm	SD-24 mm, PD-8 mm, PL-3.5 mm, threaded tapered pin	R-900, 1120, 1400 rpm, T-40 mm/min, AF-5 KN, TT-2.5°, SiC+Gr or Al_2O_3 -8:4 vol. %	Microhardness and tensile properties decreased and wear rate increased with increased R.	106
AA6061	SiC, Al_2O_3 (20 µm), Groove: W-3 mm, D-3 mm	SD-24 mm, PD-8 mm, PL-3.5 mm, threaded tapered pin	R-900, 1120, 1400 rpm, T-40 mm/min, AF-5 KN, TT-2.5°, SiC-8,6,4%, Al_2O_3-2,3,4%	Taguchi method applied to optimize parameters to improve wear and mechanical properties.	107
AA6061	SiC, Gr (20 µm), Groove: W-3 mm, D-3 mm	SD-24 mm, PD-8 mm, PL-3.5 mm, threaded tapered pin	R-900, 1120, 1400 rpm, T-40 mm/min, AF-5 KN, TT-2.5°, SiC-8,6,4%, Gr-2,3,4%	Taguchi method applied to optimize parameters to improve wear and mechanical properties.	108
AA6061	α-Al_2O_3 (95 nm), Gr (0.5 wt. %), Groove: W-1 mm, D-1.5 mm	Threaded pin profile, SD-18.5 mm, PD-4.5 mm, PL-3 mm	Wt. % of Al_2O_3-0 to10%, R-700 rpm, T-60 mm/min, AF-7 KN, TT-2°, FSP passes-1	Al/(6%Al_2O_3+0.5%Gr) composite showed superior microstructure, hardness and wear resistance.	109
AA6063	B_4C, TiB_2-10 wt.% Al, mixed with acetone and filled in Groove	SD-18 mm, PD-6 mm, PL-4.5 mm, threaded pin	R-1000 rpm for 1st 3 passes, 710 rpm for 4th pass. T-40 mm/min, TT-2°, different hybrid ratio	The composite fabricated with TiB_2 exhibited highest hardness (~137 Hv) and lowest wear rate (~0.01 mg/m) as compared to other combinations.	110
AA7075	B_4C (160, 60, 30 µm), MoS_2	SD-20 mm, PD-6 mm, PL-3 mm	R-960 rpm, T-50 mm/min, plunging speed-30 mm/min	Hybrid composite exhibited significant improvement in Microhardness, ballistic resistance and wear resistance. DOP was improved from 24 mm for 30 µm Al/B_4C composite to 12 mm for Al/(B_4C+ MoS_2).	111

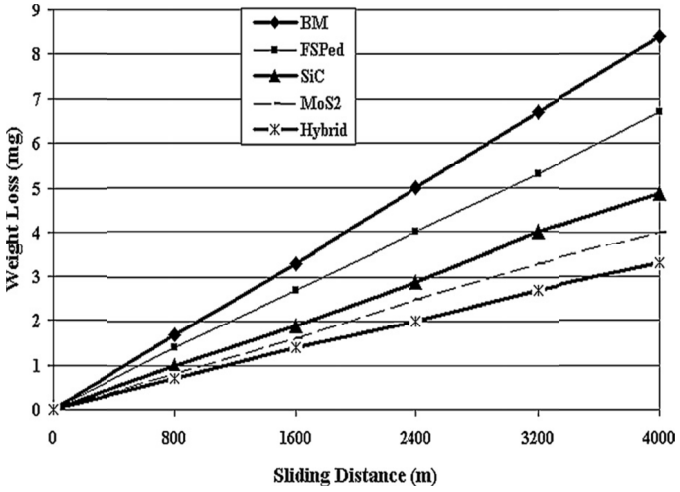

Fig. 16. Variation of weight loss vs. sliding distance (reprinted with permission from the publisher) [101]

Mostafapour and Khandani [102] fabricated AA5083/Gr/Al_2O_3 hybrid composite and reported that the Hardness and YS value were increased up to 50% Gr hybrid ratio and decreased with increased percentage of Gr. Wear rate was lower at 75% Gr hybrid ratio due to good combination of low friction coefficient, adequate hardness and presence of second phase Al_2O_3 particles. Hosseini et al. [103] used a combination of CNTs and cerium oxide (CeO_2) nano-particles in the 5083 aluminium matrix to fabricate hybrid surface composites. They illustrated that the CNT was more influencing than the CeO_2 for the improvement of mechanical properties of composite though CeO_2 also have influence on strength to some extent and provide better corrosion resistant by acting as effective cathodic inhibitor.

Rejil et al. [104] fabricated AA6360/(TiC+B_4C) hybrid surface composites and reported that the equal volume content of reinforcements exhibited lowest wear rate due to solid lubricating effect of TiC particles. Worn surface of hybrid composite depicts thin lubricating film (Fig. 17a) which results in fewer debris and broadened wear track whereas deep grooves were seen on worn surface of 100% B_4C (Fig. 17b) reinforced composite. In the later case the lubricating film was not present causing the presence of large flaky debris consequently resulting in lower wear resistance as compared with other combinations of composite [104].

Devaraju et al. [105-108] fabricated hybrid composite on 6061 aluminium alloy using SiC, Al_2O_3, and Gr as reinforcements. The microhardness of BM, AA6061/(SiC + Gr) and AA6061/(SiC + Al_2O_3) were 104, 108 and120 Hv, respectively. The average frictional coefficient of SiC + Gr reinforced composite was 0.30 in comparison of 0.36 of SiC + Al_2O_3 reinforced composite. Improvement in wear resistance occurs due to solid lubricating effect of soft Gr phase. The wear rate of both the composite increased with increasing sliding distance [105]. The increases in rotational speed results in lower wear resistance, microhardness and tensile properties for both the composites due to more heat input [106]. For Al/(SiC + Al_2O_3) composite the optimum settings for improvement in microhardness and wear properties were 1120 rpm, 6% SiC, 4% Al_2O_3 and 900 rpm, 8% SiC, 2% Al_2O_3 respectively. The responses at these settings were

132 Hv-microhardness, 189 MPa-UTS, 147 MPa-YS, 8.3-%E, and 0.002018 mm^3/m-wear rate. For Al/(SiC + Gr) composite the optimum settings for improvement in microhardness and wear properties were 900 rpm, 8% SiC, 2% Gr and 1120 rpm, 4%SiC, 3% Al_2O_3 respectively. The responses at these settings were 120 Hv-microhardness, 209 MPa-UTS, 175 MPa-YS, 9.4-%E and 0.00190 mm^3/m-wear rate. Tensile properties were found low in every combination of experiment compared to BM in both the hybrid composites [107, 108]. Prakash et al. [109] varied the wt% of Al_2O_3 from 0 to 10% and fabricated the composites. Preheating of reinforcement powders was done at 250°C for 30 minutes to improve the wettability with aluminium matrix. They reported that the hardness and wear resistance improved with increase of Al_2O_3 up to 6 wt%, beyond that it tend to decreased.

In the study of Narimani et al. [110] 100 % TiB_2 reinforced composite exhibited superior microhardness and wear resistance among various combinations of TiB_2 and B_4C due to its lower initial particle size which results in higher Orowan strengthening.

In previous study of Sudhakar et al. [99] microhardness, wear resistance and ballistic resistance of armour grade AA7075 improved using B_4C as reinforcement. They further enhanced its properties using MoS_2 as an additional reinforcement and compared properties as shown in figure 18, and 19 [111].

4. Cast aluminium alloy composites

Cast alloys contain large amount of alloying elements in comparison of wrought alloys. 3xx.x series are Al-Si+Cu or Mg alloys and possess excellent fluidity, high strength, and 131-276 MPa UTS range used mainly in automotive pistons, pumps, and electrical [59]. Salient features of single and hybrid particle reinforced composite in given in Table 7. Raaft et al. [112] found 7±1% volume fraction of reinforcements in matrix. OM images shows (Fig. 20) Gr reinforced composite exhibited higher agglomeration percent than Al_2O_3 reinforced composite, which reduces significantly with increasing rotational and decreasing traversing speed. Microhardness of composites increased more significantly with increased rotational speed and less with increased traversing speed. At higher rotational speed, Al_2O_3 reinforced composite exhibited higher microhardness (224 VHN) and lower wear rate (4.5×10^{-6} g/s).

Mazaheri et al. [113, 114] successfully fabricated A356/Al_2O_3 micro and nano composites. Un-reinforced matrix showed the general softening and hardness reduction to 67 Hv in comparison of 80 Hv of BM due to dissolution of strengthening precipitates. Addition of Al_2O_3 increased the microhardness and elastic modulus for micro, and nano composites to about

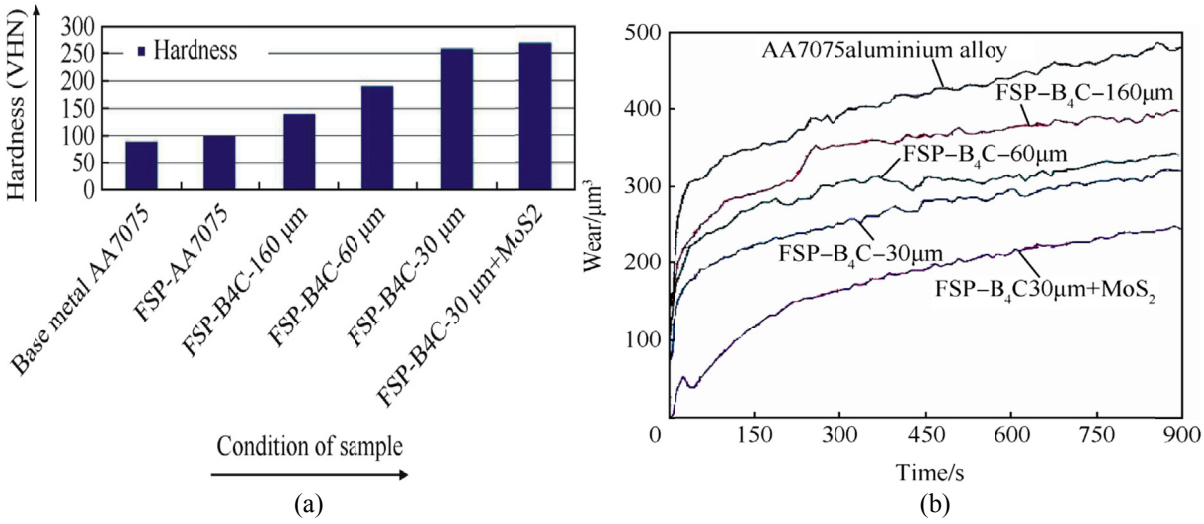

Fig.18. Comparison of (a) microhardness, (b) wear rate curves [111]

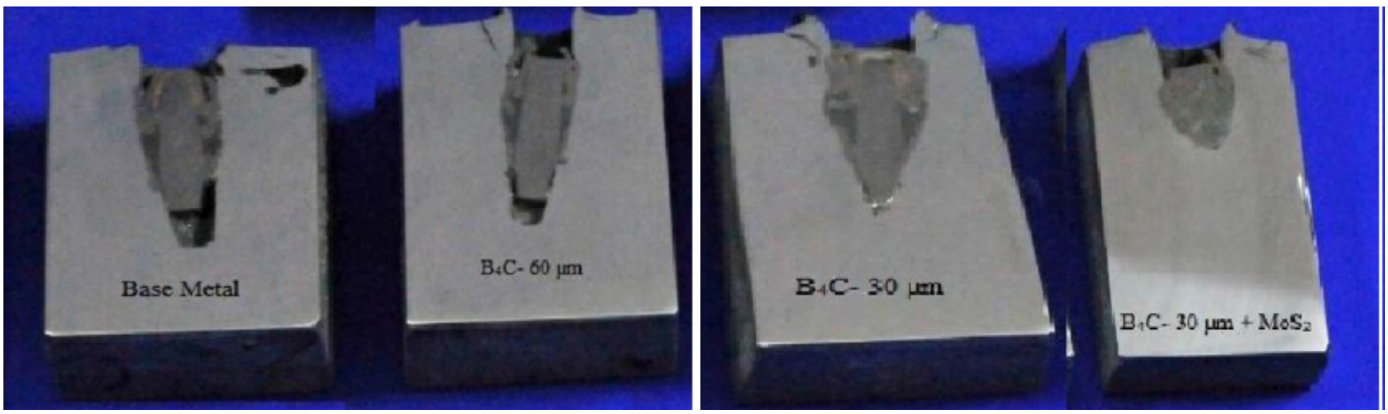

Fig. 19. Cross-sectional views of ballistic tested samples [111]

TABLE 7

A summary of single particle and hybrid reinforced cast alloy composite

Workpiece Material	Reinforcement and Strategy	Tool Specifications	Processing Parameters	Prominent Results	Reference
A390	Gr, Al_2O_3 (15-60 µm), Groove: W-4 mm, D-2 mm, powder mixed with methanol	SD-18 mm, PD-8 mm, PL-1 mm	RS-1200, 1400, 1600 rpm, TS-20,40 mm/min, TT-3°	Lower wear rate, better distribution & higher hardness achieved with increasing R. A390/ Al_2O_3 composite showed better wear resistance and higher hardness as compared to A390/Gr.	112
A356-T6	Al_2O_3 (50-100 µm and 20-40 nm), HVOF spraying	Pin with spiral groove-0.3 mm, tip end radius-4.39 mm, SD-18 mm, PD-3.6 mm, PL-4 mm	RS-1600 rpm, TS-200 mm/min, TT-2°	Composite surface layer appeared to be well bonded with no defects. Average microhardness values for A356-µ and n - Al_2O_3 composite were about 89.8±2.6 and 109.7±2.5 Hv, respectively.	113
A356-T6	Al_2O_3 (50-100 µm and 20-40 nm), HVOF spraying	Pin with spiral groove-0.3 mm, tip end radius-4.39 mm, SD-18 mm, PD-3.6, PL-4 mm	R-1600 rpm, T-200 mm/min, TT-2°	Wear mass losses of surface micro and nanocomposite specimens after 500-m sliding distance were 31, and 17.2 mg, respectively. Mode of wear was abrasive.	114
A356	SiC, Groove: W-2 mm, D-1 mm	Columnar shoulder and threaded pin, pitch-1 mm	R-1800 rpm, T-127 mm/min, Passes-2 variable AS & RS technique	Hardness improved. Spherodization of Si needles and uniform distribution of Si, and SiC were the reasons of improvement in properties.	115
A356	SiC (30 µm) & MoS_2 (5 µm) equal Vol. %, Groove: W-0.6 mm, D-3.5 mm	Columnar shoulder, threaded pin profile, SD-20 mm, PD-6 mm, PL-3.7 mm, Pitch-1 mm	R-1600 rpm, T-50 mm/min, TT-3°	SiC reinforcement improves the wear resistance of the composites. The addition MoS_2 as a hybrid reinforcement further increases it. Hybrid composite displayed higher hardness than BM, lower than A356/SiC composite.	116

89.8±2.6 Hv and 81 GPa, and 109.7±2.5 Hv and 86 GPa, respectively [113]. Wear rate and friction coefficient of BM, unreinforced matrix, micro and nano composite were found to be 101, 11.2, 62, 34.4 mg/m and 0.50, 0.51, 0.40, 0.29, respectively. The nano composite exhibited more significant wear resistance due to associated high hardness. Wear rate is inversely proportional to the hardness of material as shown in figure 21 [114].

Choi et al. [115] observed that the initial plate-like Si structure was refined after FSP. They found regularly distributed Si particles, very homogeneous microstructure and onion ring

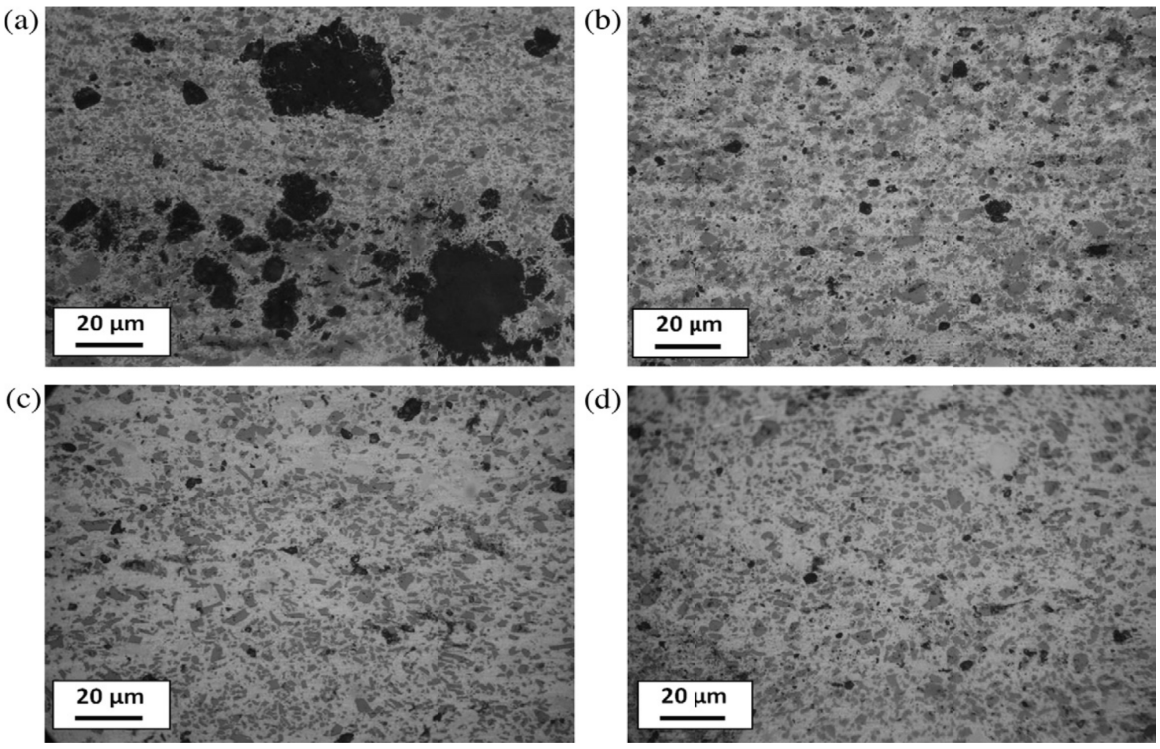

Fig. 20. OM images of (a, b) A390/graphite and (c, d) A390/ Al_2O_3 and surface composites layers FSPed at (a, c) 1200 rpm and 20 mm/min and (b, d) 1800rpm and 20 mm/min (reprinted with permission from the publisher) [112]

pattern in SZ. The hardness of BM, FSPed without SiC and with SiC specimens were found in the range of 50-65, 60-65, and 60-85 Hv, respectively.

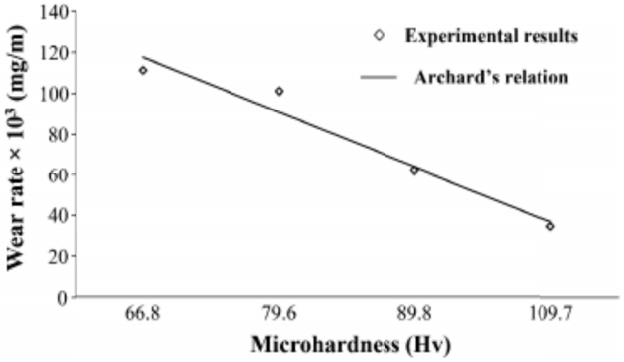

Fig. 21. Change in wear rate vs microhardness (reprinted with permission from the publisher) [114]

Alidokht et al. [116] fabricated A356/(SiC+MoS_2) hybrid composite and observed that the microhardness of the Al/SiC composite was higher than hybrid composite due to high hardness of SiC particles. They inferred from the wear test of Al/SiC composite that the hard SiC particles got detached from surface, acted as barrier against sliding, resulting in increase in friction coefficient of about 0.52-0.78 and an associated loud noise and vibration in comparison to 0.3 frictional coefficient of hybrid composite. In later, there was little noise and enhancement of the resistance to scuffing damage for hybrid composite due to formation of smooth MoS_2 rich tribo-layer.

5. Summary

FSP technique is energy efficient, environment friendly, versatile and successfully emerged as material processing technique for producing fine-grained structure, surface and bulk composites in various aluminium alloys. Intense plastic deformation affected by stirring not only mixes the particles in matrix it also shears the particles and produces fine grained and ultra fine-grained structure. The higher ratio of tool rotation speed to traverse speed and number of passes generate more heat and whip the material better to obtain homogenous distribution. In this article particular emphasis has been given to the effects of FSP parameters and various techniques on resultant microstructure and final mechanical properties of various aluminium alloys composite. The tool geometry factor is very important which influences particle dispersion. Number of FSP passes significantly influences the particle dispersion and eliminates agglomeration of reinforcements. Hard reinforcement particles along with soft particles also exhibited superior microstructure, mechanical and tribological properties. There are four possible strengthening mechanisms in MMCs- grain boundary strengthening, Orowan strengthening, dislocation induced due to the difference in coefficient of thermal expansion between matrix and reinforcement, and work hardening due to the strain misfit between the elastic reinforcing particle and the plastic matrix. Selection of efficient reinforcing particles, its volume fraction, particle delivery strategy and control of process parameters are crucial to produce defect-free microstructure. Although a number of challenges still exist and AMMC's reinforced with ceramic particles have been the subject of numerous research practitioners using various reinforcing particles, tool designs, processing parameters and techniques. For continued and further growth in applying FSP to commercial applications thermo mechanical aspects still requires clear understanding which can help in prediction of microstructure and defect free SZ.

1xxx series represents commercially pure aluminium they are non-heat-treatable, strain hardenable possess high formability, corrosion resistance and high electrical conductivity. They respond very well to the surface composite fabrication (SCF) and show up with significant increase in mechanical properties and functional characteristics. A lot of work has been reported on 1xxx series Al alloys. The 2xxx series, on the other hand, are heat treatable high strength alloys. The SCF on 2xxx series is, however, not reported as much as it is for 1xxx alloys. 2xxx series also respond to SCF with a significant improvement in hardness and wear resistance. The 5xxx, 6xxx and 7xxx series have also been investigated for the fabrication of surface composites. Several papers on 7075 are available but the maximum UTS after processing has hardly approached the strength in heat treated strength of the alloy.

5.1. Preplacement

Reinforcement particles preplaced by different techniques as outlined in the main text are commonly packed into the substrate through a FSP run with a pinless-shoulder-tool or by using a thin Al cover sheet Moreover, the surface composites have also been fabricated through a consumable shoulder tool with holes in its face through which the reinforcement particles are fed on the substrate directly. Careful examination of the available literature suggest that the groove method followed by compaction through a pinless tool before FSP is more effective and simple to implement. Other, techniques such as hole method, feeding through tool method results in increased processing time.

5.2. Creating functionally active surface

The researchers have used NiTi (shape memory alloys or SMA) particles as reinforcement to produce functional surfaces useful in sensor applications. Such surface composites were treated with post fabrication annealing that resulted in higher surface residual stress which increased with annealing temperature. Like SMAs other smart materials such as piezoelectric materials or piezomagnetic materials can also be tried as reinforcement particles. Even chemicals such as TiH_2 have also been employed, of late, to act as space holders which can be used to produce surface foams on metals.

5.3. Reinforcement particles

The researchers have tried several reinforcement materials and each produced a characteristically different effect.

- The refractory powders such as Al_2O_3, SiC, TiN, TiC, Si_3N_4, B_4C, TiB_2, ZrO_2, MoS_2 and Graphite (Gr) have been used a reinforcement particles. The particles have their own effect on the surface properties.
- The MoS_2 and Gr possess lubricating properties and hence impart better wear resistance and lesser noise. The Al_2O_3 also has lower friction, thus imparts better wear properties.
- The SiC is hard and brittle, thus increases abrasion resistance and hardness.
- The synergy may often be obtained by using a hybrid reinforcement material (combination of two or more reinforcing particles in appropriate volume fraction). This results in the improvements in several properties (e.g. wear resistance, lubrication and hardness, strengthening and wettability etc) simultaneously.
- The use of glass and carbon fibres, whiskers results in significant increase in strength and ductility both simultaneously.
- The use of multi-walled carbon nanotubes (MWCNT) results in high dislocation density and ultra fine-grains size with good interfacial bonding and wetting between MWCNTs and matrix. The microhardness of SZ, wear resistance and UTS increase significantly with the increase in volume fraction on of MWCNT but the elongation is affected adversely.

5.4. Effect of parameters

It is reported that composite layer thickness and hardness were more prominently affected by traverse rate as compared to tool rotation. The composite layer thickness reduces as the traverse speed increases. The increase in the traverse speed also has adverse effect on the bonding of composite layer with the substrate.

Various pin profiles have also been tried such as simple cylindrical, conical, threaded, conical threaded, triangular and square profiles. The threading is reported to have resulted in better mixing and particle distribution.

5.5. Effect of number of passes

The particle dispersion is usually more homogeneous in the advancing side as compared to retreating side and it improves further with increasing number of passes. FSP with multiple passes without reinforcement usually results in the grain coarsening but in presence of reinforcement particles the grain growth is restricted with the increase in the number of passes. The number of FSP passes is often used as a strategy to enhance particle distribution, but it involves lot of setup changes and inter-pass temperature rise issues. An alternate strategy has also been used by employing a simultaneous heat source e.g. electromagnetic etc. making the process hybrid. The hybrid process is reported to have resulted in significant increase in the yield.

5.6. Responses

One of the attractive features of FSP in composite fabrication is that we can control the composite area by simply changing the size and geometry of tool. A number of responses have been investigated for the FSPed surfaces which include, and not restrict to strength, hardness, wear, fatigue, corrosion resistance, size and area of the FSPed zones and particle distribution etc. Aluminium composite layer possesses high hardness, tensile strength, wear resistance and good bonding with substrate. Obviously, FSP provides all these properties in aluminium at substantially less weight than steels. Thermal conductivity and corrosion resistance of aluminium alloy have also been improved by embedding the substrate surface with GO and CeO_2, respectively. Furthermore, FSP is also utilized for imparting shape memory effect and ballistic resistance to the composite layer.

Acknowledgement

The authors wish to thank the University Grants Commission (UGC) for its financial assistance (vide sanction order No. F.3-40/2012(SAP-II)) under its SAP (DRS-I) sanctioned to Department of Mechanical Engineering, Jamia Millia Islamia, New Delhi for the project entitled “Friction Stir Welding, Ultrasonically Assisted Machining”. The authors are also grateful to the Deanship of Scientific Research, King Saud University for support through Vice Deanship of Scientific Research Chairs.

REFERENCES

[1] L.P. Borrego, J.D. Costa, J.S. Jesus, A.R. Loureiro, J.M. Ferreira, Theoretical and Applied Fracture Mechanics **70**, 68 (2014).

[2] M. Sharifitabar, A. Sarani, S. Khorshahian, M. S. Afarani, Materials and Design **32**, 4164 (2011).

[3] D. Yadav, R. Bauri, Materials Letters **64**, 664 (2010).

[4] P. Shanmughasundaram, R. Subramanian, Journal of Mechanical Science and Technology **27** (8), 2445 (2013).

[5] S. Basavarajappa, G. Chandramohan, K. Mukund, M. Ashwin, M. Prabu, Journal of Materials Engineering and Performance **15** (6), 668 (2006).

[6] W. Wang, Q.Y. Shi, H.K. Li, T. Li, Journal of Materials Processing Technology **209**, 2099 (2009).

[7] D. Pantelis, A. Tissandier, P. Manolatos, P. Ponthiaux, Materials Science and Technology **11**, 299 (1995).

[8] L.R. Katipelli, N.B. Dahotre, Materials Science and Technology **17**, 1061 (2001).

[9] C. Hu, T.N. Baker, Journal of Materials Science **30**, 891 (1995).

[10] C. Hu, H. Xin, T. N. Baker, Journal of Materials Science **30**, 5985 (1995).

[11] C. Hu, H. Xin, T. N. Baker, Journal of Materials Science **32**, 5047 (1997).

[12] T.C. Lei, J.H. Ouyang, Y.T. Pei, Y. Zhou, Materials Science and Technology **11**, 520 (1995).

[13] S.H. Choo, S. Lee, S.J. Kwon, Metallurgical and Materials Transactions A **30 A**, 1211 (1999).

[14] S.H. Choo, S. Lee, S.J. Kwon, Metallurgical and Materials Transactions A **30 A**, 3131 (1999).

[15] M. Gui, S.B. Kang, K. Euh, Metallurgical and Materials Transactions A **36A**, 2471 (2005).

[16] Y. Wang, X. Zhang, G. Zeng, F. Li, Materials and Design **21**, 447 (2000).

[17] Y. Wang, X. Zhang, G. Zeng, F. Li, Composites: part A **32**, 281 (2001).

[18] S.R. Bakshi, V. Singh, K. Balani, D.G. Mccartney, Surface & Coatings Technology **202**, 5162 (2008).

[19] R.S. Mishra, Z.Y. Ma, I. Charit, Materials Science and Engineering A **341**, 307 (2003).

[20] W.M. Thomas, E.D. Nicholas, J.C. Needham, M.G. Murch, P. Templesmith, C.J. Dawes, Friction stir butt welding: GB Patent, 9125978.8, 1991-12-06.

[21] A. Yazdipour, M.A. Shafiei, K. Dehghani, Materials Science and Engineering A **527**, 192 (2009).

[22] A. N. Siddiquee, S. Pandey, International Journal of Advanced Manufacturing Technology (2014).

[23] A.N. Siddiquee, S. Pandey, N.Z. Khan, Materials Today: Proceedings **2**, 1388 (2015).

[24] N.Z. Khan, A.N. Siddiquee, Z.A. Khan, S.K. Shihab. Journal of Alloys and Compounds **648**, 360 (2015).

[25] A.N. Albakri, B. Mansoor, H. Nassar, M.K. Khraisheh. Journal of Materials Processing Technology **213**, 279 (2013).

[26] M.K.B. Givi, P. Asadi, Advances in friction stir welding and processing, United Kingdom, Elsevier (2014).

[27] R.S. Mishra, M.W. Mahoney, Friction stir welding and processing, p. 309-350, ASM International (2007).

[28] Z.Y. Ma, Metallurgical, Materials Transactions A **39 A**, 642 (2008).

[29] Z.Y. Ma, R.S. Mishra, M.W. Mahoney, Acta Materialia **50**, 4419 (2002).

[30] I. Charit, R.S. Mishra, Materials Science and Engineering A **359**, 290 (2003).

[31] P. Cavaliere, P.P.D. Macro, Materials Science and Engineering A **462**, 206 (2007).

[32] F. Nascimento, T. Santos, P. Vilaca, R.M. Miranda, L. Quintino, Materials Science and Engineering A **506**, 16 (2009).

[33] M.M.E. Rayes, E.A.E. Danaf, M.S. Soliman, Materials and Design **32**, 1916 (2011).

[34] S. Pradeep, V. Pancholi, Material Science and Engineering A **561**, 78 (2013).

[35] C.G. Rhodes, M.W. Mahoney, W.H. Bingel, M. Calabrese, Scripta Materialia **48**, 1451 (2003).

[36] T.L. Giles, K.O. Ishi, A.P. Zhilyaev, S. Swaminathan, M.W. Mahoney, T.R. Mcnelley, Metallurgical and Materials Transactions A **40A**, 104 (2009).

[37] W.Y. Gan, Z. Zhou, H. Zhang, T. Peng, Transactions of Nonferrous Metals Society of China **24**, 975 (2014).

[38] P.B. Berbon, W.H. Bingel, R.S. Mishra, T.C. Bampton, M.W. Mahoney, Scripta Materialia **44**, 61 (2001).

[39] Y.H. Sohn, T. Patterson, C. Hofmeister, C. Kammerrer, W. Mohr, M.V.D. Bergh, M. Shaeffre, J. Seaman, K. Cho, Journal of Minerals Metals and Material Society **64**, 234 (2012).

[40] Z.Y. Liu, B.L. Xiao, W.G. Wang, Z.Y. Ma, Carbon **50**, 1843 (2012).

[41] Z.Y. Ma, S.R. Sharma, R.S. Mishra, Materials science and Engineering A **433**, 269 (2006).

[42] A.G. Rao, B.R. K. Rao, V.P. Deshmukh, A.K. Shah, B.P. Kashyap. Materials Letters, **63**, 2628 (2009).

[43] L. Karthikeyan, V.S. Senthilkumar, K.A. Padmanabhan, Materials and Design **31**,761 (2010).

[44] T.S. Mahmoud, Surface & Coatings Technology **228**, 209 (2013).

[45] J.D. M. Costa, J.S. Jesus, A. Loureiro, J.A.M. Ferreira, L.P. Borrego, International Journal of Fatigue **61**, 244 (2014).

[46] J.D. Silva, J.M. Costa, A. Loureiro, J.M. Ferreira, Materials and Design **51**, 315 (2013).

[47] S.U. Nisa, Z.A. Khan, A.N. Siddiquee, S. Pandey, Recent Advances in Mechanical Engineering 978-93-85909-51-1 (2016).

[48] Y. Hangai, K. Takahashi, T. Utsunomiya, S. Kitahara, O. Kuwazuru, N. Yoshikawam, Materials Science and Engineering A **534**, 716 (2012).

[49] R. Bauri, D. Yadav, G. Suhas, Materials Science and Engineering A **528**, 4732 (2011).

[50] C.J. Hsu, P.W. Kao, N.J. Ho, Scripta Materialia **53**, 341 (2005).

[51] G.L. You, N.J. Ho, P.W. Kao, Material Letters **90**, 26 (2013).

[52] G.L. You, N.J. Ho, P.W. Kao, Material Letters **100**, 219 (2013).

[53] G L. You, N.J. Ho, P.W. Kao, Materials Characterization **80**, 1 (2013).

[54] I.S. Lee, P.W. Kao, N.J. Ho, Intermetallics **16**, 1104 (2008).

[55] S.R. Anvari, F. Karimzadeh, M.H. Enayati, Wear **304**, 144 (2013).

[56] A. Heydarian, K.N. Dehghani, T. Slamkish, Metallurgical and Materials Transactions B **45B**, 821 (2014).

[57] N.Z. Khan, A.N. Siddiquee, Z.A. Khan, A.K. Mukhopadhyay, Journal of Alloys and Compounds (2016), 10.1016/j.jallcom.2016.11.389 (in press).

[58] G. Mathers, The welding of aluminium and its alloys, 1st Edition, Woodhead Publishing Limited, England (2002).

[59] N.R. Mandal, Aluminium welding, Woodhead Publishing Limited and Alpha Science International Limited, England (2002).

[60] M. Dixit, J.W. Newkirt, R.S. Mishra, Scripta Materialia **56**, 541 (2007).

[61] S.M. Arab, S. Karimi, S.A.J. Jahromi, S. Javadpour, S.M. Zebarjad, Materials Science & Engineering A **632**, 50 (2015).

[62] A. Kurt, I. Uygur, E. Cete, Journal of Materials Procressing Technology **211**, 313 (2011).

[63] E.R.I. Mahmoud, K. Ikeuchi, M. Takahashi, Science and Technology of Welding and Joining **13** (7), 607 (2008).

[64] E.R.I. Mahmoud, K. Ikeuchi, T. Shibayanagi, M. Takahashi, Science and Technology of Welding and Joining **14** (5), 413 (2009).

[65] M.S. Khorrami, M. Kazeminezhad, A.H. Kokabi, Materials Science and Engineering A **602**, 110 (2014).

[66] M.S. Khorrami, M. Kazeminezhad, A.H. Kokabi, Metallurgical and Materials Transactions A **46 A**, 2021 (2015).
[67] M.S. Khorrami, M. Kazeminezhad, A.H. Kokabi, Materials and Design **80**, 41 (2015).
[68] A. Thangarasu, N. Murugan, I. Dinaharan, S.J. Vijay, Sadhana **37**, 579 (2012).
[69] Q. Liu, L. Ke, F. Liu, C. Huang, L. Xing, Materials and Design **45**, 343 (2013).
[70] W. Xu, L. Ke, L. Xing, X. Zhao, Mat.-wiss. u.Werkstofftech **42** (5), 375 (2011).
[71] B. Zahmetkesh, M.H. Enayati, Materials Science and Engineering A **527**, 6734 (2010).
[72] V. Sharma, U. Prakash, B.V.M. Kumar, Materials Today: Proceeding **2**, 2666 (2015).
[73] J. Gandra, R. Miranda, P. Vilica, A. Velhinho, J.P. Teixeira, Journal of Materials Procressing Technology **211**, 1659 (2011).
[74] R.M. Miranda, T.G. Santos, J. Gandra, N. Lopes, R.J. Silva, Journal of Materials Processing Technology **213**, 1609 (2013).
[75] T.G. Santos, N. Lopes, M. Machado, P. Vilaca, R.M. Miranda, Journal of Materials Processing Technology **216**, 375 (2015).
[76] Y. Morisada, H. Fujii, T. Nagaoka, K. Nogi, M. Fukusumi, Composites: Part A **38**, 2097 (2007).
[77] M. Zohoor, M.K.B. Givi, P. Salami, Materials and Design **39**, 358 (2012).
[78] S. Shahraki, S. Khorasani, R.A. Behnagh, Y. Fotouhi, H. Bisadi, Metallurgical and Materials Transactions B **44**, 1546 (2013).
[79] A. Dolatkhah, P. Golbabaei, M.K.B. Givi, F. Molaiekiya, Materials and Design **37**, 458 (2012).
[80] C.H. Jeon, Y.H. Jeong, J.J. Seo, H.N. Tien, S.T. Hong, Y.J. Yum, S.H. Hur, K.J. Lee, International Journal of Precision Engineering and Manufacturing **15** (6), 1235 (2014).
[81] H. Izadi, A.P. Gerlich, Carbon **50**, 4744 (2012).
[82] S. Sahraeinejad, H. Izadi, M. Haghshenas, A.P. Gerlich, Materials Science and Engineering A **626**, 505 (2015).
[83] M.A. Moghaddas, S.F.K. Bozorg, Materials Science and Engineering A **559**, 187 (2013).
[84] A.S. Zarghani, S.F.K. Bozorg, A.Z. Hanzaki, Materials Science and Engineering A **500**, 84 (2009).
[85] A.S. Zarghani, S.F.K. Bozorg, A.Z. Hanzaki, Wear **270**, 403 (2011).
[86] A. Thangarasu, N. Murugan, I. Dinaharan, S.J. Vijay, Archives of Civil and Mechanical Engineering **15** (2), 324 (2015).
[87] J. Qu, H. Xu, Z. Feng, D.A. Frederick, L. An, H. Heinrich, Wear, **271**, 1940 (2011).
[88] M. Salehi, M. Saadatmand, J.A. Mohandesi, Transactions of Nonferrous Metals Society of China **22**, 1055 (2012).
[89] D.H. Choi, Y.I. Kim, D.U. Kim, S.B. Jung, Transactions of Nonferrous Metals Society of China **22**, s616 (2012).
[90] M. Saadatmand, J.A. Mohandesi, Journal of Materials Engineering and Performance **23** (3), 736 (2014).
[91] M. Salehi, H. Farnoush, J.A. Mohandesi, Materials and Design **63**, 419 (2014).
[92] K.J. Hodder, H. Izadi, A.G. Mcdonald, A.P. Gerlich, Materials Science and Engineering A **556**, 114 (2012).
[93] J.F. Guo, J. Liu, C.N. Sun, S. Maleksaeedi, G. Bi, M.J. Tan, J. Wei, Materials Science and Engineering A **602**, 143 (2014).
[94] Y. Zhao, X. Huang, Q. Li, J. Huang, K. Yan, International Journal of Advanced Manufacturing Technology **78**, 1437 (2015).
[95] D.R. Ni, J.J. Wanga, Z.N. Zhou, Z.Y. Ma, Journal of Alloys and Compounds **586**, 368 (2014).
[96] D.K. Lim, T. Shibayanagi, A.P. Gerlich, Materials Science and Engineering A **507**, 194 (2009).
[97] M. Bahrami, K. Dehghani, M. K.V. Givi, Materials and Design **53**, 217 (2014).
[98] R. Hashemi, G. Hussain, Wear **324-325**, 45 (2015).
[99] I. Sudhakar, G.M. Reddy, K.S. Rao, Defence Technology **12** (1), 25 (2016).
[100] E.R.I. Mahmoud, M. Takahashi, T. Shibayanaki, K. Ikeuchi, Wear **268**, 1111 (2010).
[101] S. Soleymani, A.A. Zadeh, S.A. Alidokht, Wear **278-279**, 41 (2012).
[102] A.A. Mostafapour, S.T. Khandani, Materials Science and Engineering A **559**, 549 (2013).
[103] S.A. Hosseini, K. Ranibar, R. Dehmolaei, A.R. Amirani, Journal of Alloys and Compounds **622**, 725 (2015).
[104] C.M. Rejil, I. Dinaharan, S.J. Vijay, N. Murugan, Materials Science and Engineering A **552**, 336 (2012).
[105] A. Devaraju, A. Kumar, B. Kotiveerachari, Transactions of Nonferrous Metals Society of China **23**, 1275 (2013).
[106] A. Devaraju, A. Kumar, A. Kumaraswamy, B. Kotiveerachari, Journal of Materials Research and Technology **2** (4), 362 (2013).
[107] A. Devaraju, A. Kumar, A. Kumaraswamy, B. Kotiveerachari, Materials and Design **51**, 331 (2013).
[108] A. Devaraju, A. Kumar, B. Kotiveerachari, Materials and Design **45**, 576 (2013).
[109] T. Prakash, S. Sivasankaran, P. Sasikumar, Arabian Journal for Science and Engineering **40**, 559 (2015).
[110] M. Narimani, B. Lotfi, Z. Sadeghian, Surface and Coatings Technology **285**, 1 (2016).
[111] I. Sudhakar, V. Madhu, G.M. Reddy, K.S. Rao, Defence Technology,**11**, 10 (2015).
[112] M. Raaft, T.S. Mahmoud, H.M. Zakaria, T.A. Khalifa, Materials Science and Engineering A **528**, 5741 (2011).
[113] Y. Mazaheri, F. Karimzadeh, M.H. Enayati, Journal of Materials Processing Technology **211**, 1616 (2011).
[114] Y. Mazaheri, F. Karimzadeh, M.H. Enayati, Metallurgical and Materials Transactions A **45A**, 2250 (2014).
[115] D.H. Choi, Y.H. Kim, B.W. Ahn, Y.I. Kim, S.B. Jung, Transactions of Nonferrous Metals Society of China **23**, 335 (2013).
[116] S.A. Alidokht, A.A. Zadeh, S. Soleymani, S. Assadi, Materials and Design **32**, 2727 (2011).